

Student thesis series INES nr 360

Sun position and PV panels: a model to determine the best orientation

Filippo Gualla

2015
Department of
Physical Geography and Ecosystem Science
Lund University
Sölvegatan 12
S-223 62 Lund
Sweden



Filippo Gualla (2015).

Sun position and PV panels: a model to determine the best orientation

Master degree thesis, 30 credits in Geomatics

Department of Physical Geography and Ecosystem Science, Lund University

Level: Master of Science (MSc)

Course duration: January 2015 until September 2015

Disclaimer

This document describes work undertaken as part of a program of study at the University of Lund. All views and opinions expressed herein remain the sole responsibility of the author, and do not necessarily represent those of the institute.

Sun position and PV panels: a model to determine the best orientation

Filippo Gualla

Master thesis, 30 credits, in Geomatics

Ali Mansourian

Department of Physical Geography and Ecosystems Science
Lund University

Roger Groth

Department of Physical Geography and Ecosystems Science
Lund University

Exam committee:

Vaughan Phillips, Lund University

Mohammadreza Rajabi, Lund University

Acknowledgements

I would like to express my gratitude to my supervisors, Ali Mansourian and Roger Groth, for their guidance and suggestions. A special thanks goes out to Britta Duve Hansen, Mats Karlsson, Thomas Åkerholm and Jonas Andreasson from Lund Kommun for their technical supports and opinions.

I would like also to thank my parents and relatives for affection and comprehension, as usual.

Finally, but only here, Giorgia... for everything.

Abstract

Sun position and PV panels: a model to determine the best orientation

This thesis presents an application, developed using the Python programming language, to define the best orientation of photovoltaic (PV) panels to make the most from the solar radiation. The development of this thesis took place at the municipality of Lund, the interested party to obtain a tool that was able to provide additional information for a better exploitation of renewable energy within the normal process of urban planning.

The developed model required data both of physical and geographical natures. The physical part, about the solar radiation, required information related to the apparent motion of the sun relative to a terrestrial observer and data, provided by the Swedish Meteorological and Hydrological Institute (SMHI), on solar energy that hits the ground surface. The geographical part instead concerned the creation of a digital surface model (DSM) from data already owned by the municipality itself and acquired by LiDAR technology.

The GIS environment, where the model has been programmed, was Quantum GIS, which is a Free and Open-Source Software (FOSS). The application is composed of a main python file and several auxiliary functions that provide interim results with the purpose of elaborating the final outputs. Starting with a list of user-defined information about the area of interest, the application provides a range of both graphical and textual results that helps to better understand the behaviour of the solar radiation on the area and therefore to provide some useful information for a more efficient use of sun energy.

The completed model was tested on a portion of the Lund municipality, characterized by a non-built area immediately next to buildings. The results have allowed understanding the annual evolution of shadows, highlighting the areas that benefit most from solar radiation, and consequently how the shadows affect the average amount of kWh/m² of sun energy that reaches the ground. The most useful results for the study purposes concern the identification of the best angle of orientation of a PV system. The last annual output suggests how areas not hampered by shadows, casted from tall structures, require values of azimuth of 180 degrees. Instead, the monthly outputs suggest the best values of azimuth for those areas where 180 degrees is not the optimal orientation.

The application proposed here is based on a simple physical model, it is developed with non-proprietary software and uses data that are becoming more and more available on the net and finally provides results within a reasonable time. However a model, as such, can always be reconsidered starting from its foundation and, therefore, always be improved. During the implementation process some aspects that can encourage its further development have already been identified.

Keywords: GIS, Python modelling, LiDAR, DSM, Solar radiation, Orientation angle, Photovoltaic systems

Table of contents

1	INTRODUCTION	1
1.1	Background	1
1.2	Research objectives.....	2
1.3	Thesis structure.....	3
2	MODELS AND PHYSICAL BACKGROUND	5
2.1	Solar radiation models.....	5
2.1.1	Numerical methods.....	5
2.1.2	Solar potential urban-oriented models.....	7
2.2	Sun position equations.....	8
2.2.1	Sunrise and sunset	9
2.2.2	Sun elevation and sun azimuth angles.....	12
2.3	Solar radiation and surfaces	15
2.3.1	Sun radiation and the atmosphere of Earth	15
2.3.2	Tilted surfaces	16
2.4	PV panel structure	17
3	DATA, TOOLS AND METHODOLOGY	19
3.1	Data	19
3.1.1	Lund municipality data: from LiDAR/LAS file to DSM.....	19
3.1.2	SMHI data	21
3.2	Tools: FOSS - Free and Open-Source Software.....	22
3.2.1	QGIS 2.8.2 “Wien”.....	22
3.2.2	Python 2.7.....	23
3.2.3	Modules: GDAL and LAStools	24
3.3	Methodology.....	25
4	PYTHON MODELLING IN QGIS ENVIRONMENT	27
4.1	Model description.....	27
4.1.1	The main script: MAIN.py	29
4.1.2	Function “Cast_01Rec_AzimRec”	33
4.1.3	Function “kW_Shadow”.....	34
4.1.4	Function “Best_Azimuth”	34
4.2	Brief description of model outputs	38
5	RESULTS: A CASE STUDY	41
5.1	Study area	42
5.2	Yearly analysis	44
5.2.1	Shadow casting.....	44
5.2.2	Average kW of sun energy hitting the surface	45
5.2.3	Best yearly azimuth angle: 180 degrees	47
5.3	Monthly analysis	49
5.3.1	Text outputs.....	51
5.4	Changing the percentage range	52
5.5	Changing the input DSM extension	54

6	DISCUSSION	59
6.1	Model implementation.....	59
6.2	Model output results	61
6.2.1	Yearly results.....	61
6.2.2	Best azimuth and monthly results.....	62
6.3	Further insights on the theoretical background of the model.....	63
7	CONCLUSIONS AND FURTHER DEVELOPMENTS	65
	REFERENCES.....	67
	APPENDICES	72
	LIST OF PUBLICATIONS.....	73

List of abbreviations

AMSL	Above Mean Sea Level
DEM	Digital Elevation Model
DSM	Digital Surface Model
ESRI	Environmental Systems Research Institute
FOSS	Free and Open-Source Software
GDAL	Geospatial Data Abstraction Library
GIMP	GNU Image Manipulation Program
GIS	Geographic Information System
GNU	GNU's Not Unix
GPS	Global Positioning System
GUI	Graphical User Interface
JDN	Julian Day Number
JRC	Joint Research Centre
LAS	LASer file format
LiDAR	Light Detection And Ranging
OOP	Object-Oriented Programming
OSGeo	Open Source Geospatial Foundation
PDF	Portable Document Format
PV	PhotoVoltaic
QGIS	Quantum GIS
SMHI	Sveriges Meteorologiska och Hydrologiska Institut
TIF	Tagged Image File format
TOC	Table Of Content
TXT	Text file extension
UTC	Coordinated Universal Time
WGS	World Geodetic System (latest revision: WGS 84, aka WGS 1984, EPSG:4326)

List of figures

Figure 2.1: Spherical coordinates: radial distance r , inclination angle θ (theta) and azimuth angle φ (phi)	12
Figure 2.2: The two angles considered to define the Sun position.....	12
Figure 2.3: Apparent motion of the Sun across the sky	14
Figure 2.4: Angles defining the relationship between the incoming beam radiation and a tilted surface.....	16
Figure 3.1: Monthly averages of global irradiance ($\text{kWhm}^{-2} \text{ day}^{-1}$) from SMHI data	21
Figure 3.2: QGIS logo.....	22
Figure 3.3: Python logo.....	23
Figure 3.4: An overview of the methodology.....	26
Figure 4.1: Diagram's symbology.....	29
Figure 4.2: Diagram of the "for loop" of the main script "MAIN.py"	31
Figure 4.3: Diagram of the last steps of the main script "MAIN.py" (out of the loop).....	33
Figure 4.4: Diagram of the first steps of the script "Best_Azimuth.py" involving the "if statements"	36
Figure 4.5: Graphical explanation of the key analysis performed by Best_Azimuth.	38
Figure 5.1: Simulation study area. A) Location within the town of Lund; B) Satellite image	43
Figure 5.2: Study area DSM (elevation in meters), slope and aspect	43
Figure 5.3: 3D visualization of the study area from the "point cloud"	44
Figure 5.4: Yearly shadow casting percentage.....	45
Figure 5.5: Yearly average kWh/m^2 of sun energy	46
Figure 5.6: Average daily kWh/m^2 (representative day).....	47
Figure 5.7: Areas where yearly best azimuth is always 180 degrees.....	48
Figure 5.8: December best azimuth (JDN 344) intermediate output	48
Figure 5.9: Monthly best azimuth	50
Figure 5.10: A different monthly output due to different percentage ranges	54
Figure 5.11: New resized input DSM.....	55
Figure 5.12: Monthly best azimuth computed on the new input DSM.....	57

List of tables

Table 2.1: Input data for Sunrise/Sunset Algorithm.....	9
Table 2.2: Input data for Sun Position Algorithm	13
Table 3.1: Specification for LiDAR flight session.....	20
Table 4.1: The “.py” files containing the scripts of the entire Python model.....	28
Table 4.2: Functions relationships within the Python model	28
Table 4.3: Representative days from Technical standard UNI 8477-1, 1983	29
Table 4.4: [A] a layer of the 12 stored in the dictionary and [B] the best azimuth 180 layer	32
Table 4.5: Input variable definition.....	34
Table 4.6: Reclassification rules of the Day_Percentage_Shadow raster	35
Table 5.1: Information output from the text file “2015_MAIN_Analysis_LOG.txt”.....	41
Table 5.2: Technical information about the simulation and input variables	42
Table 5.3: Original LAS files used to extract the study area.....	43
Table 5.4: Best azimuth angle values for each percentage within the percentage range (55-85%)	51
Table 5.5: Shadow percentage per representative day (text file output).....	52
Table 5.6: Best azimuth values for 45-90% and 35-95% simulations across the 12 representative days	53
Table 5.7: Best azimuth angle values, computed on the new input DSM, for each percentage within the percentage range (55-85%)	56

1 INTRODUCTION

Nowadays administrations, from national down to local level, must be able to estimate revenues and costs of each solution identified during the decision-making process. The impact of a strategy varies greatly depending on the territory on which it is implemented (Lamie et al. 2012). This spatial dependence makes essential a geographical approach to the analysis of many phenomena that can have an important role in the management of a territory (Santos et al. 2014). Increasing the efficiency and energy saving is one of the points that plays a key role in plans for local government and for this reason more and more often is taken into consideration the production of energy through the use of photovoltaic panels (PV panels).

The municipality of the town of Lund, like many others, has already started to integrate its services with tools aimed at the quantification of usable solar energy and has shown interested to deepen the subject. In this master thesis we tried to develop a GIS tool that would provide additional information on how to make the most of solar energy from some data already available within the municipality itself.

1.1 Background

The production of energy from renewable resources has become a major issue, decisive, considering the environmental problems and the social implications that we have with the use of fossil fuels (Tait 2014; Urry 2014). From this point of view, the solar energy is factual unlimited and with the least impact on the environment, evaluating all structures necessary for its exploitation (Solangi et al. 2011). In addition, over recent years, PV panels are becoming more efficient and new technologies are being tested and introduced (Lukač and Žalik 2013). However to get an energy production that comes as near as possible to the maximum achievable it is not an easy task. The PV panels must be placed and oriented according to certain requirements in order to be efficient. Variables such as the type of panels, the tilt and the orientation angle must be chosen carefully.

A detailed analysis of the entire process of electricity production, from when the sun's rays hit the Earth ground, is a complicated task that requires taking into account many variables, both physical and technological. In this project, the municipality of Lund did not want to get a result so wide, but rather obtain intermediate outputs that may be immediately useful on a practical level. From 2009 to present, new data about the surface of the territory of Lund has been collected and the municipality was interested in analysing this new data in a GIS environment to obtain additional information that could be used in the normal decision-making process, particularly with regard to the design of new buildings within the urban planning office duties. One of the key points was to develop a model to understand which should be the best orientation of a new building or

a new PV panels array to get the highest solar irradiation. The angle of orientation is called technically “azimuth angle” and even if it is more desirable to set it at 180 degrees (facing the south, in the northern hemisphere) some factors can lead to a modification of the azimuth angle: first of all shading effects (Martinez-Rubio et al. 2015).

In literature it is possible to find many articles that present models designed to estimate accurately the amount of solar energy that hits the ground at any given time using very different approaches from “numerical weather models” (Shamim et al. 2015) to neural network analysis (AL-Naimi et al. 2014). Similarly there are many reports dealing with optimal angles of inclination and orientation for PV panels as function of the latitude (Gopinathan et al. 2007; Bakirci 2012; Yadav and Chandel 2013). These studies are rarely contextualized within a GIS environment where instead is predominant the spatial analysis about solar radiation (Hofierka and Suri 2002; Araya-Muñoz et al. 2014; Santos et al. 2014), as in the municipality project started in the 2009 and mentioned above. The effect of the shadows (“shadow casting”) instead is often taken into account in the 3D modelling in architecture, where this aspect is important for the design of the buildings. In this context architectural software is preferred rather than one dedicated to GIS.

1.2 Research objectives

The office of urban planning of the municipality of Lund has to take decisions, among others, regarding plans for the construction of new buildings. A variable to be considered is how to orient a future building to maximize the production of solar energy through PV panels. The main objective of this study is to provide an answer to this question by creating a simple model within a GIS environment, considering all aspects reported in the previous section. To achieve this result, we wanted to use as much as possible open source software (FOSS) since it offers several advantages for example in terms of costs and implementation. Following this philosophy, the model was built with Python, within Quantum GIS (QGIS). We will cover a little more in detail about the software in Section 3.2.

Within the mentioned main objective, the specific objectives are:

- to test the behaviour of the model;
- to define, in the area of interest, the shadow casting in relation to the apparent motion of the Sun (both daily and yearly):

the apparent motion of the sun relative to a point on the Earth surface creates and casts shadows on the ground. During the course of a year, as a function of natural or man-made structures, some areas will be more in the shade of others. This result wants to define, as a percentage value, how much an area is shaded during the course of a whole year;

- to provide an yearly estimation of the sun energy hitting the ground on average according to some historical data:

the sun emits a thermal radiation of $6,66 * 10^7$ W/m², but the one that comes to Earth is a very small part. This output wants to show an average annual input of energy per unit of area that actually reaches the ground starting from historical data about solar radiation;

- to define the areas where the yearly best orientation (best azimuth) is 180 degrees no matter which month is considered:

from a definition provided by the Cornell University (Astro.cornell.edu 2015), “the azimuth of an object is the angular distance along the horizon to the location of the object. By convention, azimuth is measured from north towards the east along the horizon”. The “Best yearly azimuth angle” is a layer that will show those portions of the surface where, throughout the course of the year, the best orientation of a building or a PV panel array will be always at 180 degrees of azimuth, i.e. southward;

- to identify the variation of values in best azimuth (out of areas showing 180 degrees) within a representative day (we will discuss later about the concept of “representative day” in Section 4.1):

for each month (or representative day) azimuth values for those areas not covered by the previous result will be provided. Here will be shown azimuth angles, specifically calculated, that do not necessarily have value 180.

1.3 Thesis structure

The thesis report is structured as follow. In the second Chapter, “Models and Physical Background”, is briefly proposed the theory that allows the study of the sun’s position with respect to an observer on the earth and literature about the models of solar radiation. In addition, the mathematical formulation to calculate times of sunrise and sunset as a function of latitude and day of the year is shown. In the Chapter 3, “Data, Tools and Methodology”, the input data from Lund municipality will be present together with a brief introduction about the software involved. In the following Chapter 4, “Python Modelling in QGIS Environment”, there is a detailed description of the model and the assumptions behind it. Chapter 5, “Results: a case study”, shows the results coming from our model applied to a study area. In the last two Chapters, “Discussion” and “Conclusions and Further Developments”, we present a discussion of the results and some consideration about them and finally our conclusion about the model and also some further developments which came out during the work-process.

2 MODELS AND PHYSICAL BACKGROUND

This Chapter describes a perspective about knowledge and models in the literature and the physical concepts behind the developed model presented in this report. In the first part, some relevant studies and numerical methods will be briefly presented together with a few examples of solar potential urban-oriented models. In last sections the physics involved in this model will be explained: it is part of the navigational and positional astronomy and studies on solar radiation. We will introduce the basis for calculating the position of the sun relative to a terrestrial observer with known coordinates. With regard to solar radiation, it will be taken into analysis summarily its propagation through the atmosphere of the Earth. Finally a brief introduction to the technology of photovoltaic panels will be provided.

To determine the exact position of the sun is important for many applications, but especially for those regarding solar energy (Chong et al. 2009). There are various algorithms to calculate the solar position and new ones come out in order to improve the accuracy (Grena 2012). Often these algorithms are very complicated for direct use in many applications, for this reason in this thesis approximate equations will be used. With minimal loss of accuracy, these formulas allow direct calculation of the position of the sun at a given time and the conditions. All formulas set out below come from the “Almanac for Computers” (Doggett et al. 1990) and the “Photovoltaic Education Network” (Pveducation.org 2015a).

2.1 Solar radiation models

Many models developed to estimate the solar radiation on the ground are used in the field of energy use. These models have been also implemented into GIS environment, releasing several toolset.

Computational solar radiation models are many and the most complete date back about 25 years ago. These studies are divided into two branches: numerical methods and solar potential urban-oriented models (Freitas et al. 2015). Below some of the models that can be found in literature are presented, including the model developed for the municipality of Lund through the project “Solkartan” (Krafringen.se 2015a).

2.1.1 Numerical methods

These methods are essentially simulation software that analyse the solar energy balance on a given surface from physical formulations and taking into account the possible obstacles that might exist between the path of the solar energy and the surface itself.

These models consider almost always of all three types of solar radiation (for details see Box 2.1, page 15).

SolarFlux

SolarFlux, born in 1993, was developed on the platform Arc Info (Hetrick et al. 1993). As input about the surface, it required a GRID file containing values of elevation, latitude and atmospheric transmission. This tool was used to obtain as output the total direct and diffuse radiation, the direct sun duration and, in addition, a “fish-eye” projection of sky obstructions. SolarFlux has subsequently influenced the development of another model designed by Kumar and colleagues where the user can enter additional information on cloud cover (Kumar et al. 1997).

ArcGIS Solar Analyst

Solar Analyst is an ArcView GIS extension (Fu and Rich 1999) developed in the C ++ language which can help the user to calculate the influence of the topography of an area on the solar radiation. The model requires as input the geographical location of the area of interest, elevation, orientation and finally, as physical data, the atmospheric transmission and some meteorological measurements (air and soil temperature and soil moisture). However this model has shown how the techniques, often used to generalize some physical data required by the models, are not sufficiently accurate to determine the radiation patterns. This model provides as output different maps of solar radiation.

r.sun

The tool “r.sun”, now available as a module for Quantum GIS (Section 3.2), has been developed since 1997 as GRASS GIS-based model (Hofierka and Suri 2002). The model aims to estimate the solar radiation both when the sky is clear and in overcast atmospheric conditions. This module requires several parameters but not all of them are mandatory (Grass.osgeo.org 2015). The most important parameters are raster layers for terrain, latitude, turbidity and clear-sky index. In one of the previous versions, the tool worked in two different modes providing two different set of outputs: 1 - instant time mode and 2 - daily mode. This option allowed the user to set the time interval of the analysis. In the last available version, the user seems to be allowed to work only with the second mode (daily). Outputs are raster maps of the area showing the beam, diffuse, ground reflected and global irradiance. The model can be used in very different time and space scales. As for Solar Analyst however, some physical parameters often prove to be unreliable and hard to find (e.g.: Linke turbidity factor).

ESRA

ESRA (European Solar Radiation Atlas) is a clear sky model, programmed in C language, capable to derive irradiation information from satellite images (Rigollier et al. 2000). This model requires, as r.sun, the Linke turbidity factor and the elevation of the site. The result is an estimation of the diffuse clear-sky irradiation. This model was validated through ground measurements provided by different ground stations.

2.1.2 Solar potential urban-oriented models

The analysis of solar radiation contextualized in an urban environment has led to the creation of more complex models for the study of the physical phenomenon. The complexity of the models is related to the analysis of solar radiation on the facades of buildings that, in a 3D model of the ground, represent a sharp discontinuity of the values of elevation from the ground. Actually not all the developed models take into account the facades of the buildings and some others represent the buildings as simple parallelepipeds without considering for example the slope of the roofs.

Skelion

Skelion is a CAD (Computer-aided design) plugin-based model for Google SketchUp (Skelion 2013). This plug-in estimates the electrical power output of PV panels previously set on some given buildings or structures. It can consider obstacles that could cast shadows on the energy elements. The estimation of the electrical production comes from some available databases and the final result is in form of a report. With this tool the information about building facades is lost.

v.sun

This module, available for Quantum GIS and implemented in GRASS GIS environment, processes 3D vector data representing urban environments (Hofierka and Zlocha 2012). This GIS-based model has some new ways of analysing the 3D city models and vertical surfaces just as the facades of buildings. This module is based on the existing module *r.sun* but with the addition of the capability to analyse 3D vector objects. The developers have introduced a new algorithm for the analysis of the relationship of the shadows among objects: the surfaces that make up the objects are broken down into smaller elements in order to better represent the fragmentation caused by the casting of the shadows. As for the module *r.sun*, also *v.sun* provides values relative to the beam, diffuse and reflected radiation but as a kind of attribute for each element of the polygons representing the buildings.

SOL

SOL is another GIS-based model, developed with MatLab (Matrix Laboratory), that aims to identify which parts of a building are the best for the installation of PV panels and, more generally, the areas available for this purpose (Catita et al. 2014). SOL requires different input data: a solar radiation model specific for roofs, ground and vertical surfaces, a 3D city model, a DEM (Digital Elevation Model) and meteorological information associated with the area of interest. The model returns the irradiance value for each surface taken into account in the input data.

Finally, some developed models are the basis for free online applications which provide estimations of solar radiation to the ground from different parameters. Some are provided by private (Solar Electricity Handbook 2015), others are sites of non-profit organizations (Pveducation.org 2015b) and research centres as the European Commission in-house science service Joint Research Centre (JRC; Re.jrc.ec.europa.eu 2015).

For a complete review of the models the recent work of Freitas and colleagues can be consulted (Freitas et al. 2015). The last model presented below is the result of a joint project for the creation of a map of solar radiation for the entire municipality of Lund.

Solkartan Project: Lund model

The municipality of Lund, together with Kraftringen, Lunds Tekniska Högskola (LTH) and Solar Region Skåne, has made available online to users an urban-scale solar cadastre map (Kraftringen.se 2015a). This map is the result of a project started in 2009 with the collection of elevation data with laser-scan technology (Kraftringen.se 2015b). The user can get information on which would be the total value of annual solar radiation incident on a roof across the entire municipality.

The model requires primarily information regarding the location of the roofs of the buildings in the territory. This information has been gathered through a laser scanning, both by helicopter and airborne, and then the 3D model of the buildings was created. In this phase of the project the 3D model was not yet usable: it was necessary to “clean” the data by eliminating all those temporary structures, such as cranes, which could influence the final result. Subsequently, with the aid of ArcGIS (ESRI software) and the Solar Analyst tool an estimate of direct solar radiation was made and obtained the map, this has been cut using as a mask composed by polygons representing the roofs of buildings (Hedén 2013). Finally, in order to make information accessible to non-expert users, the values of solar radiation for every roof were categorized into “not suitable” for PV panels installation, “almost acceptable”, “good” and “very good” together with a colour scale (respectively grey, green, yellow and red). The user, by clicking on a specific roof, gets information about it: a graph representing how much energy could be produced and the annual solar radiation on that roof. However the results presented in this map are not absolute. Weather variations can lead to different values than those calculated. The aim of this map was to provide an overview on the sun energy potentially exploitable.

The following sections will present the physical assumptions and formulas used to create the model proposed in this report.

2.2 Sun position equations

To calculate the position of the sun relative to the horizon it is necessary to know where the observer is and when: spatial and temporal information are required. The position is always defined by latitude and longitude. The time is determined by the day and time of interest. As will be seen in Chapter 4, the model must be provided by several hours in the course of a single day to perform the analysis.

The day is defined by the year, month and day number. In order to define different times within the given day, hour of sunrise and sunset as well as latitude and longitude must be known. Latitude and longitude (expressed in decimal degrees, WGS84) can be found easily on the web or on the field with an ordinary GPS device while to accomplish the computation of the hours of sunrise and sunset, the equations provided by the

“Almanac for Computers” will be used. Once all the information on the observer is given we proceed to calculate the position of the sun relative to the horizon.

2.2.1 Sunrise and sunset

The equations to calculate sunrise and sunset will be taken within the function “RiseSetSpan” of the model. The inputs are listed in the Table 2.1:

Table 2.1: Input data for Sunrise/Sunset Algorithm

Input		Meaning
year, month, day number		Date of Sunrise/Sunset
Latitude and Longitude (decimal degrees, WGS84)		Location of the Sunrise/Sunset
Zenith:		
Official	= 90 degrees 50'	The point of the celestial sphere that is directly opposite the nadir and vertically above the observer. (Definition from http://www.merriam-webster.com)
Civil	= 96 degrees	
Nautical	= 102 degrees	
Astronomical	= 108 degrees	
Local offset (UTC offset)		It is the difference in hours and minutes from UTC for a particular place and date

The angles in the formulas have to be considered as expressed in radians and the value of Zenith to consider is the “Official”. Longitude is positive towards East and negative for West. The procedure is as follows:

1. Calculate the Julian Day Number (JDN) of the day of the year. JDN is the integer assigned to a whole solar day in the Julian day count starting from noon Greenwich Mean Time, with Julian day number “0” assigned to the day starting at noon on January 1, of the selected year:

$$N1 = \text{floor} \left(275 * \frac{\text{month}}{9} \right)$$

$$N2 = \text{floor} \left(\frac{\text{month} + 9}{12} \right)$$

$$N3 = 1 + \text{floor} \left[\frac{\text{year} - 4 * \text{floor} \left(\frac{\text{year}}{4} \right) + 2}{3} \right]$$

$$JDN = N1 - (N2 * N3) + \text{day} - 30$$

Equation 2.1: JDN calculation

2. Convert the Longitude to hour value and calculate the time:

$$LongHour = \frac{Longitude}{15}$$

$$\text{For sunrise time: } t = JDN + \left(\frac{6 - LongHour}{24} \right)$$

$$\text{For sunset time: } t = JDN + \left(\frac{18 - LongHour}{24} \right)$$

Equation 2.2: Time approximation for Sunrise and Sunset

3. Sun's mean anomaly calculation "M":

$$M = (0,9856 * t) - 3,289$$

Equation 2.3: Sun's mean anomaly

4. Sun's true Longitude "L":

$$L = \{M + [1,916 * \sin(M)] + [0,02 * \sin(2 * M)] + 282,634\} - 360$$

Equation 2.4: Sun's true Longitude

5. Sun's right ascension "RA", setting of the ascension in the same quadrant as L, ascension conversion into hours:

$$RA = \tan^{-1}[0,91764 * \tan(L)]$$

Equation 2.5: Sun's right ascension

$$Lquadrant = \left[\text{floor} \left(\frac{L}{90} \right) \right] * 90$$

$$RAquadrant = \left[\text{floor} \left(\frac{RA}{90} \right) \right] * 90$$

$$RA = RA + (Lquadrant - RAquadrant)$$

Equation 2.6: Ascension in L quadrant

$$RA = \frac{RA}{15}$$

Equation 2.7: RA conversion into hours

6. Calculate sine and cosine of Sun's declination:

$$\sin Dec = 0,39782 * \sin(L)$$

$$\cos Dec = \cos(\sin^{-1}(\sin Dec))$$

Equation 2.8: Sun's declination

7. Sun's local hour angle "H" and conversion into hours:

$$\cos H = \frac{[\cos(Zenith) - (\sin Dec * \sin(Latitude))]}{[\cos Dec * \cos(Latitude)]}$$

If $\cos H > 1$ the Sun never rises at the given location

If $\cos H < -1$ the Sun never sets at the given location

For sunrise time: $H = 360 - \cos^{-1}(\cos H)$

For sunset time: $H = \cos^{-1}(\cos H)$

$$H = \frac{H}{15}$$

Equation 2.9: Sun's local hour angle

8. Calculate the local mean time of sunrise/sunset:

$$T = H + RA - (0,06571 * t) - 6,622$$

Equation 2.10: Local mean time for sunrise and sunset

9. Adjust the local mean time back to UTC (Coordinated Universal Time):

$$UT = T - LongHour$$

Equation 2.11: Adjustment of the local mean time according to the UTC

10. Convert the UT value to the local time zone (defined by Latitude and Longitude):

$$LT = UT + localOffset$$

Equation 2.12: Adjustment of the UTC local mean time according to the local time zone

From these equations it is possible to get the hours of sunrise and sunset for a given day of the year to a given position.

2.2.2 Sun elevation and sun azimuth angles

Between the hours of sunrise and sunset the sun makes its apparent motion across the sky constantly changing its position.

The position of an astronomical object is defined within a spherical coordinate system by three numbers (Figure 2.1): i) the radial distance “ r ” between the object and a fixed origin (or an observer), ii) the angle “ θ ” measured from a fixed Zenith direction and called polar angle or inclination angle (often this angle is replaced by its complementary angle “ α ” - alpha - that is called elevation angle) and iii) the azimuth angle “ φ ” (Morse and Feshbach 1999). It is already been

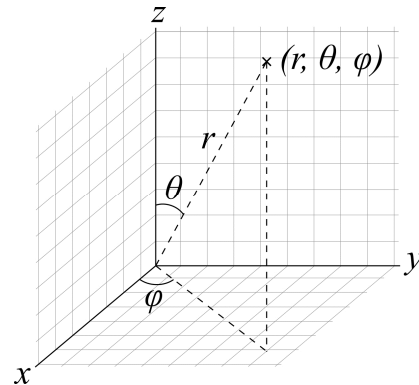


Figure 2.1: Spherical coordinates: radial distance r , inclination angle θ (theta) and azimuth angle φ (phi) (Picture from <https://en.wikipedia.org>)

mentioned the azimuth angle (Subsection 1.2) but its more formal definition is as follows: it is the angle defined by the orthogonal projection of the object on a reference plane that passes through the origin (or observer) and is orthogonal to the Zenith and that is measured from a fixed reference direction on that plane.

In this report the elevation angle “ α ” will be considered instead of the inclination angle: when this angle is at the horizon its value is zero. The azimuth angle value is 0 degrees northward, 90 degrees eastward, 180 degrees southward and 270 degrees westward (Figure 2.2). The radial distance here is of no importance for the calculations and is considered to be infinite as the solar rays are considered to be parallel to each other.

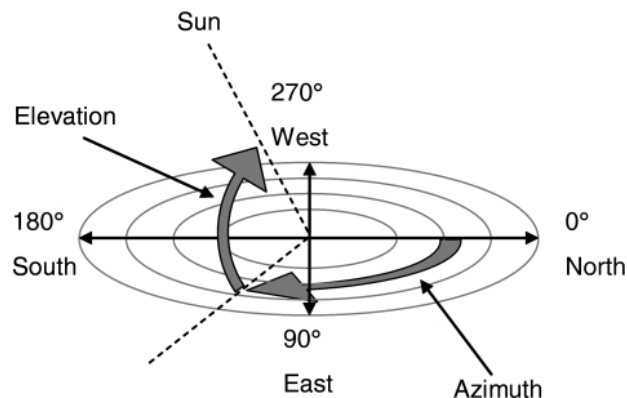


Figure 2.2: The two angles considered to define the Sun position: elevation angle α and azimuth angle φ (Picture from Zijffers et al. 2008)

The equations to calculate azimuth angle φ and elevation angle α will be taken within the function “SunPos” of the model. These two angles are the keys to orient properly a solar power plant. The inputs are listed in Table 2.2.

Table 2.2: Input data for Sun Position Algorithm

Input	Meaning
year, month, day number	Date of interest
Latitude and Longitude (decimal degrees, WGS84)	Location of interest
Local Time “LT”	Any time in between from sunrise and sunset
Local offset (UTC offset)	It is the difference in hours and minutes from UTC for a particular place and date

As before, when trigonometric functions sine and cosine are called, the angles in the formulas have to be considered as expressed in radians. The procedure is as follows:

1. Compute the JDN as shown in Equation 2.1
2. Compute the Local Standard Time Meridian “LSTM”:

$$LSTM = 15 * localOffset$$

Equation 2.13: Local Standard Time Meridian (“15” is in degrees)

3. Compute the Equation of Time “EoT” in minutes

$$B = \left(\frac{360}{365}\right) * (JDN - 81)$$

$$EoT = 9,87 * \sin(2 * B) - 7,53 * \cos(B) - 1,5 * \sin(B)$$

Equation 2.14: Equation of Time

4. Time Correction factor “TC” in minutes:

$$TC = 4 * (Longitude - LSTM) + Eot$$

Equation 2.15: Time Correction factor

5. Local Solar Time “LST”:

$$LST = LT + \left(\frac{TC}{60}\right)$$

Equation 2.16: Local Solar Time

6. Hour Angle “HrA”:

$$HrA = 15 * (LST - 12)$$

Equation 2.17: Hour Angle (“15” is in degrees)

7. Sun's declination angle “ δ ” (delta):

$$\delta = 23,45 * \sin \left[\frac{360}{365} * (JDN - 81) \right]$$

Equation 2.18: Sun declination angle (“23,45” in degrees)

8. Elevation angle α and Azimuth angle φ :

$$\alpha = \sin^{-1}[\sin(\delta) * \sin(\text{Latitude}) + \cos(\delta) * \cos(\text{Latitude}) * \cos(\text{HrA})]$$

Equation 2.19: Elevation angle

$$\varphi = \cos^{-1} \left[\frac{\sin(\delta) * \cos(\text{Latitude}) - \cos(\delta) * \sin(\text{Latitude}) * \cos(\text{HrA})}{\cos(\alpha)} \right]$$

Equation 2.20: Azimuth angle

With these equations the position of the Sun is determined across a day at any given time (LT). The sun traces an imaginary arc in the sky above the horizon, as shown in the following figure (Figure 2.3).

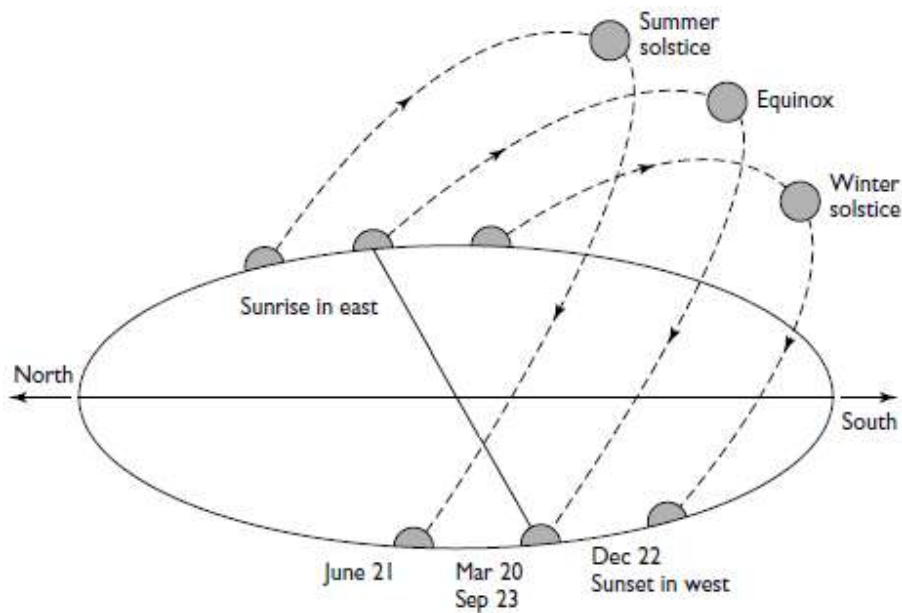


Figure 2.3: Apparent motion of the Sun across the sky

(Picture from <http://www.cse.iitk.ac.in/users/amit/books/gingerich-2005-nicolaus-copernicus-making.html> and modified by the author with GIMP 2.8)

At mid-latitudes of the northern hemisphere, during the winter time the Sun rises south of due east and sets south of due west while in summer time it rises north of due east and sets north of due west crossing two times a day the east-west line.

2.3 Solar radiation and surfaces

In this section some fundamentals are presented in order to understand what is meant by “solar radiation” and especially how it interacts with Earth’s atmosphere and what are the units of measure involved. Finally, some parameters that have to be considered when solar radiation strikes an inclined surface as a PV panel will be presented. This theory is based on Chapters 1 and 2 of the text “Solar engineering of thermal processes” (Duffie and Beckman 2006).

2.3.1 Sun radiation and the atmosphere of Earth

Because of the eccentricity of Earth’s orbit, the Earth-Sun distance varies by about 1.7%. However, the radiation emitted by the Sun and its spatial relationship with the Earth leads to a nearly fixed value of intensity of solar radiation outside the Earth’s atmosphere. The solar constant I_{sc} is the energy received on an imaginary unit area normal to the direction of propagation of the solar radiation per unit time at the average distance Earth-Sun outside the atmosphere. The value of I_{sc} is 1387 W/m^2 . The intensity of solar radiation hitting a surface is called “irradiance” or “insolation”, I_0 , and its unit of measure is W/m^2 or kW/m^2 (units of power per unit area). The total amount of energy from the solar radiation is measured in J/m^2 (units of energy per unit area) and is called “irradiation”, H .

The intensity I_{sc} is an average value which actually varies throughout the year also due to extra-terrestrial sources of variation. For this project it is useful instead to see how this value changes once solar beams interact with the atmosphere. Beam radiation (Box 2.1), before reaching the Earth’s surface passes through the atmospheric mass and this scatters and absorbs part of the solar energy. “Rayleigh scattering” takes place when the molecules of gas are a lot smaller than the wavelength of the radiation. This phenomenon is important because around half of the incoming radiation is scattered and lost to outer space. Part of the radiation remain reaches the surface from all directions as diffuse radiation (Box 2.1). When particles in the atmosphere are larger than the wavelength of the radiation, the scattering process is called “Mie scattering”. The amount of radiation involved in this last scattering process is dependent on location and weather condition. The sum of all types of solar radiation (defined in Box 2.1) is defined as “Total Solar Radiation” or “Global Radiation” on the surface. The rate at which the energy coming from the Sun is incident on a surface unit area is the irradiance and each kind of the previous radiations can be defined by it with the appropriate subscript.

Box 2.1: DEFINITIONS

Beam (or direct) radiation is the amount of Sun radiation reaching a plane on the Earth’s surface without having been scattered by the atmosphere.

Diffuse radiation is the portion of Sun radiation hitting a plane on the ground after its direction has been modified by the molecules in the atmosphere.

Reflected radiation is defined by direct and diffuse radiation beams that, after having hit the ground surface, are reflected onto the plane.

In summary, the global irradiance on the ground, on a disposed surface, varies from instant to instant, from season to season and from one geographical location to another.

2.3.2 Tilted surfaces

The relationship between the beam radiation and a plane with a given position on the Earth's surface can be defined geometrically with different angles. Going into detail of this relationship, the mentioned plane can be considered as a surface that produces energy when hit by solar radiation. The angular positions involved in this relationship (Figure 2.4) are the following and here are all expressed in degrees:

1. Latitude ϕ : position north or south from the equator; $-90^\circ(\text{S}) \leq \phi \leq 90^\circ(\text{N})$;
2. Sun Declination δ : position of the Sun at solar noon (Sun on the local meridian) with respect to the equator plane; $-23,45^\circ(\text{S}) \leq \delta \leq 23,45^\circ(\text{N})$;
3. Tilt angle β (or slope): angle between the surface and the horizontal; $0^\circ \leq \beta \leq 180^\circ$ ($\beta \geq 90^\circ$, the surface faces downward);
4. Surface azimuth angle γ (or orientation angle): projected the normal to the surface on a horizontal plane, γ is the deviation of the this projection from the local meridian; usually it is defined in the interval $-180^\circ/180^\circ$ (with 0° towards south) but in this report, also for the surface azimuth will be used the following scheme: 0 degrees northward, 90 degrees eastward, 180 degrees southward and 270 degrees westward;
5. Hour angle ω : the eastward/westward angular displacement of the Sun from the local meridian (5° hour; negative in the morning, positive in the afternoon);
6. Angle of incidence Θ_s : angle between the beam radiation on the surface and the normal to that surface.

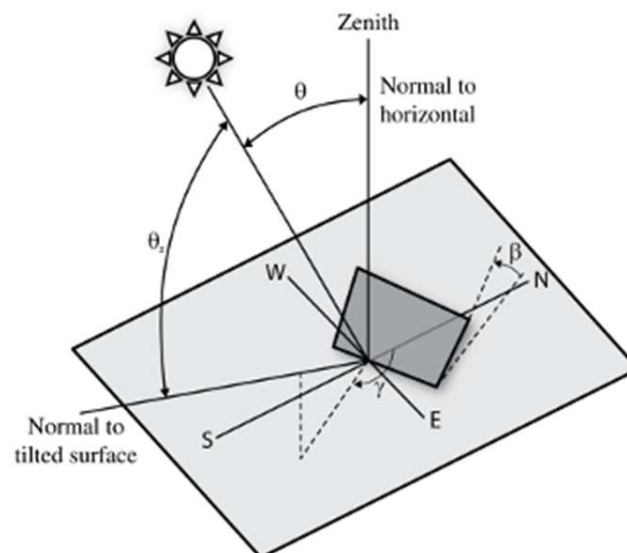


Figure 2.4: Angles defining the relationship between the incoming beam radiation and a tilted surface (Picture from Gulin et al. 2013, modified by the author with GIMP 2.8)

Tilt and orientation angles (azimuth), β and γ respectively, are the two main variables affecting the efficiency of a PV panel (Jafarkazemi and Saadabadi 2013). Sometimes, due to the technical properties of a PV panel, it is not possible to set the tilt or the orientation angles according to the current sun position (e.g. solar tracking system). In this peculiar situation the best solution is to identify the best value of these parameters trying to maximize the incidence of the solar radiation. In this report we are going to focus only on the azimuth of a solar surface (γ) and the best orientation of a solar surface is obviously southward. Nevertheless sometimes buildings or areas are located in a way that prevents the south orientation; in this case it is necessary to change the orientation.

2.4 PV panel structure

Here it will be explained very briefly how a PV surface is structured. This short introduction will be useful to understand some of the assumptions of the model presented below.

Photovoltaic technology has as its basic unit the semiconductor solar cells that, connected together (usually 36 connected in series), form a module or panel. It is very important to stress that the connection is in series and not in parallel: this solution has very important implications in case of partial shading of the panel. The solar cells are made of amorphous silicon or bulk silicon and usually the second type is that which lasts more over time. Since 2008 approximately, PV panels with solar cells of about 150 mm in diameter are produced: that means that a single PV panel has a surface of at least 0,81 m² or more. A series of PV panels connected together, in series or parallel, forms a PV array (El Saeid Mustafa 2012; Pveducation.org 2015c)

A PV panel operates whenever the solar rays hit it, producing electrical energy, and more the solar radiation is intense and the panels are directly stricken (the rays are orthogonal to the surface) more electricity will be produced.

3 DATA, TOOLS AND METHODOLOGY

The development of the program laid the groundwork on the fact that input data would be a Digital Surface Model (DSM) and a series of historical data about solar energy reaching the surface on the area of interest. Starting from that data, we developed the tool using mainly an open-source GIS software and an open-source programming language together with some modules and extensions still available from the web to perform some additional tasks.

3.1 Data

3.1.1 Lund municipality data: from LiDAR/LAS file to DSM

Around every 5 years the Lund Municipality performs a flight throughout the whole municipality territory to collect data on the elevation of the land. By means of a light detection and ranging survey (Lta.cr.usgs.gov 2015), an airborne laser scanning LiDAR collects data on elevation changing providing, as first output, a LAS file (Asprs.org 2015) to store the information.

LiDAR technology

LiDAR is a remote sensing technology composed by a laser, a scanner and optics and a position and navigation system receiver unit (GPS). This system emits pulsed and intense light beams and measures the time that the reflected beam takes to be detected by the sensor. These values are used to evaluate ranges or distances to the objects lying on the ground. For each point collected, the system computes the couple of coordinates (x for the latitude and y for the longitude) and the elevation value (z).

One of the most important characteristics of this technology is the ability to rapidly collect measurements of the Earth's surface: the result is a so called "point cloud", a highly dense collection of georeferenced points with information about elevation. This raw data can be subsequently manipulated to build a very accurate model of the surface. Usually the elevation accuracy spans from 10 to 20 centimetres for recent data and the point density per square meter can reach the number of 15 (National Oceanic and Atmospheric Administration 2012; Oceanservice.noaa.gov 2015). Airplanes and helicopters can be used to carry LiDAR instruments. For areas with a small extent, as the Lund municipality, deploying instruments on a helicopter is the favourite choice to get a higher point density.

LAS file format

The output from a LiDAR survey is stored within a file with a LAS extension (Laser file) which is the industry standard format for LiDAR data. The American Society of Photogrammetry and Remote Sensing (ASPRS) provides the specification of this public file format. Actually, the LAS file is supposed to store generally a point cloud dataset and LiDAR falls into this category. Hardware vendors usually provide also the software to put data in LAS format. The main aim of ASPRS was to create a common format for point cloud data.

The LAS file is defined as follow (American Society of Photogrammetry and Remote Sensing 2013):

1. Public Header Block: it contains generic information as the total number of points or the min/max values of x , y and z ;
2. Variable Length Records (VLRs; optional): it can contain different types of data as metadata or projection information;
3. Point Data Records;
4. Extended Variable Length Records (EVLRs; optional): it is identical to a VLR but it can store larger data content.

In the Appendix 1 it is provided an example of a LAS file opened as text file where is possible to see some of the information usually stored into this kind of format.

Lund Municipality surface model

Lund Municipality did two flight-sessions, one the day 2015/01/19 and the other the day 2015/02/15 to produce a model of the surface of the whole municipality territory. The company which performs the collection of the data was Blom Sweden AB. In the Table 3.1 there is some specification of the laser-scanning sessions (Blom Sweden AB 2015).

Table 3.1: Specification for LiDAR flight session

System	TopEye 533
Flight Elevation	300 – 600 m (<i>variation due to weather condition</i>)
Laser Pulse Frequency	100 kHz
Point Density	12 points / m ²
Reference System	SWEREF99 13 30
Total Collected Points	5 880 000 000

The point cloud has been stored in 2009 LAS files, each defining a tile that covers, on average, an area of 500m x 500m; tiles close to the border of the municipality have a lower extension. Each 500 x 500m tile has on average 3 million points but tiles covering urban areas can double this value.

3.1.2 SMHI data

The Swedish Meteorological and Hydrological Institute (SMHI – Sveriges Meteorologiska och Hydrologiska Institut) provides historical data on global radiation starting from January 1, 1980 to December 31, 2000 (Smhi.se 2015). Data were produced with support from the Swedish Radiation Protection Authority, Strålsäkerhetsmyndigheten, and the Swedish Environmental Agency, Naturvårdsverket (Strang.smhi.se 2015).

From the SMHI web page the entire time series of global irradiance (Wh/m^2) has been downloaded, in the form of text files. The time resolution has been monthly, daily and hourly (expressed in UTC - Coordinated Universal Time), but only the latter has been used for practical purposes. To extract data it is possible to enter the latitude and longitude of the area of interest, in this case latitude 55,70 N and longitude 13,22 E. This data will be used to calculate the average annual value of energy, due to solar radiation, hitting the Earth's surface (Subsection 4.1.3).

The raw text file, obtained with hourly temporal resolution, shows for each row: year, month, day, UTC time (from 0 to 23 with step 1) and the value of global irradiance recorded. It is necessary that the data are stored in this order to be properly processed by the appropriate function "Month_Avg_Solar_Rad_H" called by the main program (Subsection 4.1.1).

Below (Figure 3.1) the average daily solar radiation (in units of $\text{kWh/m}^2\text{day}$), produced from the hourly values, is reported. The computation regarded the entire time series (21 years).

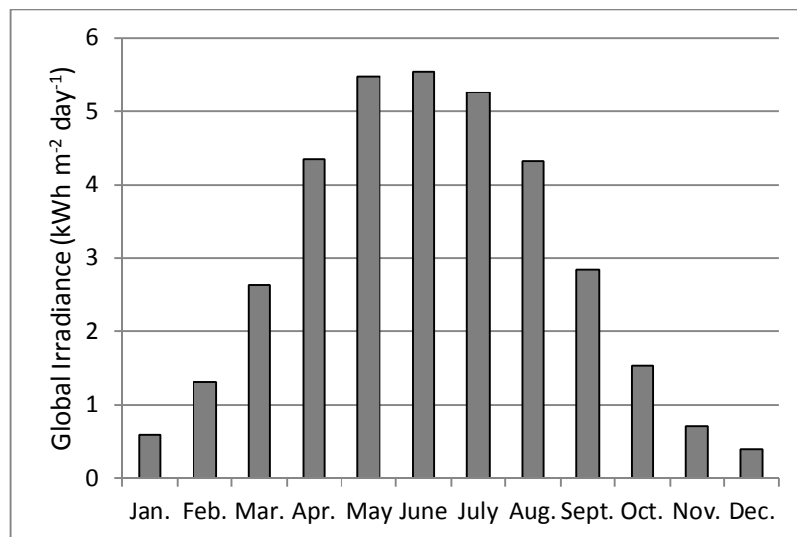


Figure 3.1: Monthly averages of global irradiance ($\text{kWhm}^{-2} \text{day}^{-1}$) from SMHI data. Area coordinates: Lat. 55,70N and Long. 13,22E

3.2 Tools: FOSS - Free and Open-Source Software

The model described in this report has been created trying to use as much as possible open-source software: FOSS. The acronym stands for “Free and Open-Source Software” and it is a word which refers to that software that is non-proprietary, a large number of people can work on it and it can be shared without any cost (Gnu.org 2015). In this light, many governmental organization, agencies and administrative bodies are increasingly choosing to use open software. The reasons for switching to these software are easy to understand, for example: i) the money that can be saved without having to pay for a proprietary software license, ii) it is possible to act directly on the code and it is therefore easier to identify anomalies and vulnerabilities, iii) there are extensive online communities that can solve problem and provide help and advices, iv) are customizable (Cassell 2009).

On this basis, and considering the necessity of having to move within a GIS environment and to be able to code, the model has been developed taking advantage of QGIS version 2.8.2 “Wien” (Qgis.org 2015a) and Python 2.7 Release (Python.org 2015a). In addition modules and packages available for free have been used to perform some tasks. These libraries will be described in detail in Subsection 3.2.3.

3.2.1 QGIS 2.8.2 “Wien”

QGIS is an Open Source GIS software licensed under the GNU General Public License. This software is an official project of the Open Source Geospatial Foundation (Qgis.org 2015b). It is a flexible GIS software which supports several raster, vector and database formats and provides many functionalities. Like most of the GIS software, QGIS presents a Table of Contents, TOC, showing the loaded layers and the largest area of the software is occupied by the map overview. There is a standard menu system and many customizable button rows displaying some tools. A status bar provides information on the spatial extent, scale and current coordinates of the cursor. It is possible to open an additional table to show all the GeoAlgorithms already loaded in the current QGIS version.



Figure 3.2: QGIS logo
(Picture from <https://commons.wikimedia.org>)

All figures in this report have been created using the “Print Composer” of QGIS. The “Print Composer” provides layout and printing capabilities. It allows the user to add elements such as maps, text labels, images, legends, scale bars or basic shapes. The created layout can be printed or exported to image formats or PDF (Docs.qgis.org 2015).

In addition, like any GIS software, also QGIS provides several modules, called “GeoAlgorithms”, to perform various tasks. In the model very common functions in GIS environment have been used. Modules already included within QGIS, like SAGA or GRASS, allowed to reclassify the values of a raster (SAGA reclassifygrsvalues or GRASS r.reclass), filter it (SAGA majorityfilter) or perform Map Algebra (SAGA

rastercalculator). A feature not so common, but very useful for the model, has been “analytical hillshading” with the method “Ray Tracing” belonging to SAGA package.

SAGA Analytical hillshading: Ray Tracing method

Generally a hillshading algorithm is based on the angle between the surface and the incoming light beams. The option “Ray tracing” can calculate and show the shade of objects in a digital surface model according to two angle parameters: Sun azimuth and Sun elevation from the horizon. This option is in fact the basis of one of the major functions, “Cast_01Rec_AzimRec”, developed for this project (Subsection 4.1.2).

Graphically, it is possible to appreciate the operation of this method in Figure 4.5C. From C1 to C3 the casting shadows on the ground vary in location according to the variation in values of azimuth (see values in legend) and elevation (C1: 5,77 degrees, C2: 13,16 degrees and C3: 10,56 degrees).

3.2.2 Python 2.7

Python is a programming language widely used and it is becoming more and more popular. It allows a high level of programming and emphasizes the concept of “readability” of the code. Among its several strengths, Python supports object-oriented programming paradigm and offer an extensive range of standard libraries.



Figure 3.3: Python logo
(Picture from

<https://www.python.org/community/logos>)

Some aphorisms included the document “PEP 20 - The Zen of Python” summarize the philosophy of Python (the complete document can be found at this web address: <https://www.python.org/dev/peps/pep-0020/>):

Explicit is better than implicit.

Simple is better than complex.

Complex is better than complicated.

Readability counts.

Special cases aren't special enough to break the rules.

Python has appeared for the first time in 1991 and have been released several versions until arriving at 3.4.3. In recent years it has become increasingly popular due to several advantages that distinguish it over other programming languages. Python is a simple and essential language that can be defined as a “pseudo-code”: it allows the user to focus on the planning and the resolution of the problem rather than having to spend time to the complexity of the language itself. In relation to this point, the basic syntax is very simple, for example for statement grouping is used a simple indentation rather than curly braces or begin-end blocks. A very simple syntax allows a greater ease of approach

for beginners of programming and this aspect has done nothing but facilitate its spread. As the title of this section says, Python is an example of FOSS and this has led to the birth and the development of a large community that is constantly improving the language and supports anyone who needs help. Another strength of Python is its portability: all programs written by a user in this language can be run on different platforms without having to undergo any changes. For example it can be used on Linux, Windows, Macintosh and even on PlayStation. Thanks to its versatility, Python is often embedded in other software products as scripting language.

As said, Python supports object-oriented programming (OOP). Object-oriented programming involves bringing in a limited area of the source code (called “class”) the declaration of the data structures and procedures that operate on them. Classes, therefore, represent abstract models, which are invoked at runtime to instantiate objects for the class invoked. Objects have attributes (data) and methods (procedures) as defined by the respective classes.

Python has a number of standard libraries that help the user in various aspects such as the use of expressions, database management, web browser, e-mail, cryptography or Graphical User Interface (GUI): this is the so-called “batteries included” philosophy of Python. There are also libraries dedicated to specific fields of knowledge such as scientific computing, computational biology or astronomy.

Python, like all programming languages, has different data-types and for the implementation of the model presented here was made extensive use of the data types “list” and especially of the “dictionaries”. The elements of a dictionary appear in a comma-separated list. Each entry contains a “key” (a sort of index) and a “value” separated by a colon: keys are unique while values may not be (Tutorialspoint.com 2015).

The QGIS software provides a built-in “Python Console” where the user can run scripts written in Python syntax or use this programming language stand-alone.

3.2.3 Modules: GDAL and LAsTools

Free software is often accompanied by modules and libraries of tools that can be downloaded from the net to extend the capability of analysis of the software itself.

Geospatial Data Abstraction Library: GDAL

GDAL is a library, used by several software including Python, which allows manipulating geospatial raster and also vector data (Gdal.org 2015). It is released under an Open Source license by the Open Source Geospatial Foundation (OSGeo).

Tools for LiDAR data: LAsTools

LAsTools is a collection of batch-scriptable command line tools to process LiDAR data (rapidlasso GmbH 2012). Although it is a free download, some of the tools work correctly only if purchased a license otherwise the tool runs but provides results with

showy artefacts. However the tool to convert a LAS file into a DSM (“las2dem”) is one of those that work correctly without license.

In the model, the raw input geographic data was a LAS file, from which the DSM was created using “las2dem”. The tool reads the file and after having entered a few parameters, including the “pixel size” to define the resolution of the output raster (1m in this case), the DSM is created and ready to be used. The tool “lasinfo” provides some information about a LAS file (e.g. Appendix 1). “lastxt” instead creates a text file which lists all the collected points (x , y , and z) stored in the file. Another useful tool is “lasview” which displays the points in 3D allowing the user to have an immediate idea of the contents of the file without having yet processed it.

3.3 Methodology

The methodology that has led to the realization of the model is shown in Figure 3.4. First, a meeting with some members of the municipality of Lund took place to define in detail the purpose of the project according to their requirements. Information on solar radiation models and the formulas for calculating the position of the sun, during its apparent motion with respect to a point on the earth, have been collected through a literature search. In addition the literature search has allowed deepening the physical knowledge about solar radiation and formulas that define its relationship with surfaces located on the ground. At this stage an architect from the faculty of Engineering (Energy and Building Design) at the Lund Tekniska Högskola (LTH) was interviewed about the model proposal. After the interview outcome, the literature review on models already available has been deepened and especially about how these models deal with sun apparent motion.

The next step was the collection of raw data. During the initial meeting, some members of the municipality expressed the intention to use LiDAR data in their possession within the project. Along with this dataset, data about solar radiation were downloaded from the SMHI website. After the collection stage, data has been prepared in order to be properly inserted into the program. A digital surface model (DSM) was created starting from LiDAR data and the SMHI dataset was revised in order to be better handled by the program. The preparation phase of the data took place in parallel with the initial part of the system design. Then the program was developed and implemented by programming in Python.

The program was run several times, during the development phase, to test the different functions that make it up. After that, the final version of the program was ready for testing. This version was continuously tested by varying different input parameters and to produce results.

Finally, evaluations of the program behaviour were made and the results, that the different tests have produced, were analysed.

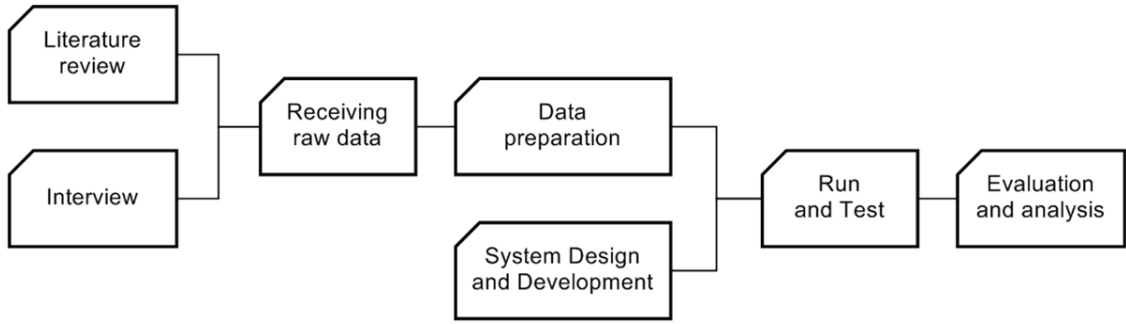


Figure 3.4: An overview of the methodology

4 PYTHON MODELLING IN QGIS ENVIRONMENT

This chapter explains how the model has been programmed and the functions of which it is composed. The physical assumptions at its base have been presented in Chapter 2 and the analysis assumptions will be presented here and discussed in Chapter 6.

4.1 Model description

The programming of the model is part of the thesis project as objective to respond to the request of the municipality of Lund. The model aims to provide some results in the production of energy from solar radiation, trying to develop useful outputs in urban planning. Starting from the data described in the previous chapter and from the input area considered (DSM), the model provides:

1. the annual shadowing percentage (output layer);
2. the average amount of kWh/m² per day which hits the ground (output layer);
3. the best yearly azimuth angle (γ): 180 degrees area (output layer);
4. the monthly best azimuth (γ) values (output layers);
5. some “txt” files gathering analysis data and information (text files).

The model consists of a file “.py” containing the main script and 12 modules (“.py” files) in which are located from one to three specific functions to perform a specific task. The 13 “.py” files are shown in the Table 4.1.

The main program can be saved anywhere, instead modules must be placed in the subdirectory “Plugins” of QGIS.

The Table 4.2 shows the relationships between the various functions, as they are called up by the various scripts.

**Table 4.1: The “.py” files containing the scripts of the entire Python model.
“M” stands for “major function” and “m” for minor function**

Name	Type	Content (functions)
MAIN.py	Main script	---
Best_Azimuth_180_Month.py	Module	Best_Azimuth_180_Month (M)
Best_Azimuth_INmonth.py	Module	Best_Azimuth (M)
Best_Azimuth_Year.py	Module	Best_Azimuth_Year (M)
Cast_01Rec_AzimRec.py	Module	Cast_01Rec_AzimRec (M)
Date_Time_Setting.py	Module	ConvenTime (m) Month_Name (m) JDN (m)
Formula_Reclassification.py	Module	Reclass_Formula (m)
kW_Shadow.py	Module	kW_Shadow (M)
Month_Avg_Solar_Rad.py	Module	Month_Avg_Solar_Rad_H (m) Month_Avg_Solar_Rad_M (m) Month_Avg_Solar_Rad_D (m)
Month_Shadow.py	Module	Month_Shadow (M)
RasPixelAreaProp.py	Module	RasPixelAreaProp (m)
RiseSetSpan_Time.py	Module	RiseSetSpan (m)
SunPos.py	Module	SunPos (m)

Table 4.2: Functions relationships within the Python model

1 st Level	2 nd Level (called functions)	3 rd Level (called functions)
Main Script	Month_Avg_Solar_Rad_H	SunPos
	RiseSetSpan	
		SunPos
	Cast_01Rec_AzimRec	ConvenTime Month_Name JDN
	Month_Shadow	Reclass_Formula
	kW_Shadow	Reclass_Formula RasPixelAreaProp
	Reclass_Formula	
	Best_Azimuth	Reclass_Formula Month_Name
		Reclass_Formula SunPos
	Best_Azimuth_Year	ConvenTime Month_Name JDN
	Best_Azimuth_180_Month	

Before proceeding with the description of the program it must be introduced the concept of “representative day”. The model takes some time to carry out the analysis and, having it run over a full year, the total execution time would be too long. It is chosen to reduce the number of computations at the monthly level: the model does not run for each day but each month is represented by a single day. When the monthly average solar radiation has to be calculated, some reference days (Renno and Petito 2013) can be used and they can be found in the Technical Standard UNI 8477-1, 1983. We chose to use these representative days (Table 4.3) instead of opting for days chosen randomly. So within this report, “representative day” and “month” may be considered interchangeable concepts.

Table 4.3: Representative days from Technical standard UNI 8477-1, 1983

Month	Day	Year Day (n)
January	17	17
February	16	47
March	16	75
April	15	105
May	15	135
June	11	162
July	17	198
August	16	228
September	15	258
October	15	288
November	14	318
December	10	344

This section is structured as follow: in the first subsection the main script will be described briefly and in the subsequent subsections the “major” functions (Table 4.1) will be then described more in detail. In the Figure 4.1 is presented the symbology used to draw the diagrams shown in this chapter.

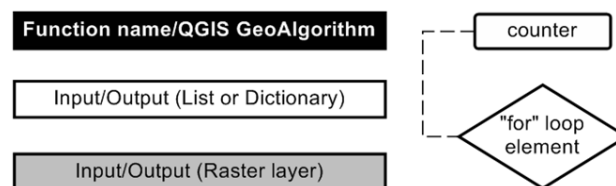


Figure 4.1: Diagram's symbology

4.1.1 The main script: MAIN.py

The main program consists of a single “for loop” in which some functions are called up and run for every representative day. Completed the full loop, run 12 times, the script proceeds with additional operations that essentially use the interim results created daily in the for loop to provide the output layers both annual and monthly. In addition, both in the main script and in some functions, the various text files outputs and the necessary folders to store intermediate data are created.

The user enters within the main script some basic information as: the main folder where to store all the results, the referring year to perform the analysis, the path where to find the input DSM and the SMHI data text file, latitude and longitude in WGS84 of the area of interest and the values of maximum and minimum for the range of percentage (more details in Subsection 4.1.4). Below is a short description of the steps in order of performance.

1. The function “Month_Avg_Solar_Rad_H” elaborates the SMHI input data to compute, within a specific day and specific hour, the mean of the kWh/m². Then it creates a dictionary where, for every representative day (key) is connected another dictionary (dict. value) and these sub-dictionaries have the “hour of the day” as key and the computed average of kWh/m² as value.

The program now comes into the main “for loop” through the 12 representative days.

2. The function “RiseSetSpan”, based on the physical assumptions described in Section 2.2, provides the time of sunrise, sunset and hours of light for the representative day considered within the loop. In addition it provides the floor value of the hours of light and a so-called “step” value which is the ratio between the hours of light and the floor value of these hours.
3. The “major” function “Cast_01Rec_AzimRec” (details in Subsection 4.1.2) requires as input the DSM and the representative day information from step 2. It returns two dictionaries as output and both has as key the sun azimuth and a raster layer as dictionary value. Even the stored raster are the same but with a little difference in the cell values: both has “0” for the area where light reaches the ground but in the raster stored in first dictionary the cells where the light is shaded by some structure get “1”, in the second those cells get the exact value of azimuth of the sun casting shadows.
4. “Month_Shadow” is the second “major” function recalled. This function receives the information about the representative day and the first dictionary from step 3 and returns two kinds of results: a raster layer and a list. The layer shows the daily percentages of shadows computed through the layers stored in the input dictionary. This layer is stored in a main dictionary as value coupled with the current representative day as key. The list stores all the percentage values derived from the previous analysis of this function (e.g.: Table 5.5).

This raster is produced by means of SAGA rastercalculator (Map Algebra). Rastercalculator requires, among the inputs, the formula which describes the type of operation to be performed and the function “Reclass_Formula” provides this equation written in the proper way. The function sums the layers stored in the input dictionary and divide the result by the number of layers.

5. “kW_Shadow” (details in Subsection 4.1.3) is now run and it has as input the representative day, the first dictionary from step 3 and the result of the function Month_Avg_Solar_Rad_H run in the beginning, out of the loop. The function returns a raster storing, for each cell, the proper kWh/m² per day value hitting the surface. The main program here starts to fill in another main dictionary where the key is the representative day and the value is the raster just produced.
6. Last major function called is “Best_Azimuth” (details in Subsection 4.1.4). The output layer shows, for each area defined previously by a certain percentage of shadow, the best orientation of a building or a PV panel array. The list contains all

the best azimuth values computed for the previous result. These two results are stored in two different main dictionaries as values, coupled with the current representative day (key).

At this point the main for loop is ended and once it went through all the 12 representative days, the main script goes ahead to produce the main yearly and monthly outputs. The Figure 4.2 shows the diagram of the script described above.

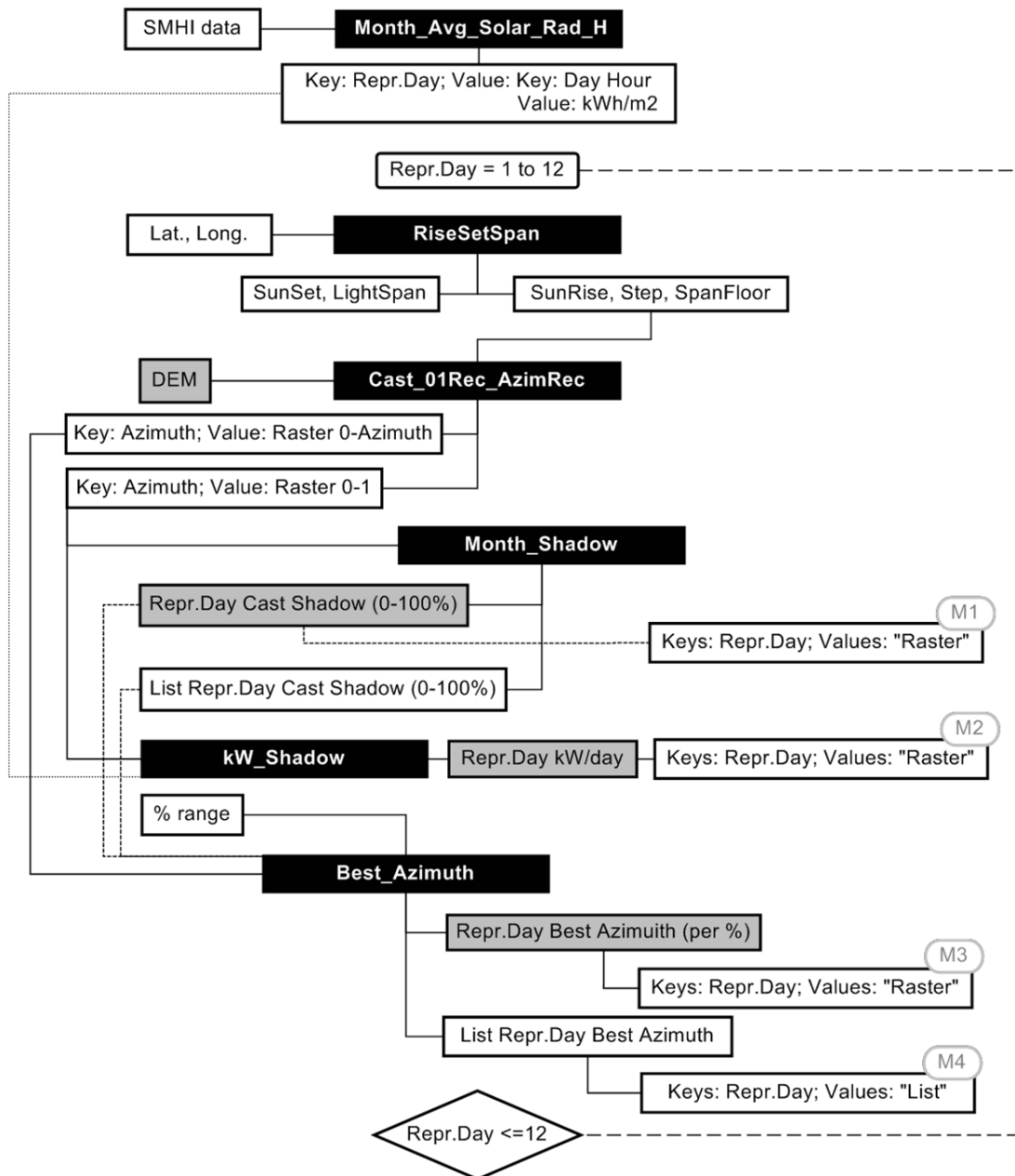


Figure 4.2: Diagram of the “for loop” of the main script “MAIN.py”. All the functions inside the loop have also as input variable the day, month and year of the representative day. “M” defines the outputs that will be passed and used in the next steps of the program, out of the loop.

7. The first main output layer shown in the TOC is the yearly “shadow casting” percentage. This result is computed by means of “SAGA rastercalculator”. The script sums all the layers stored in the main dictionary filled by Month_Shadow (step 4) and divides the result by 12.
8. The next step is analytically identical to the previous. Layers stored in the second main dictionary (step 5) are sum together via “SAGA rastercalculator”. In this way the main output storing the yearly average amount of kWh/m² hitting the ground is produced and shown in the TOC.
9. The function “Best_Azimuth_Year” takes the layers stored in the main dictionary from step 6 and computes the layer showing the areas where the best azimuth is always 180 degrees through all the months of the year. The function invokes “SAGA raster calculator” to sum the layers and divide by 12.

Finally a filter tool (SAGA majorityfilter; radius=2) is applied to the previous result to delete isolated pixel storing a different value compared to the surroundings. This assumption will be discussed in Chapter 6. Now where the raster value is 180, the best azimuth through all the year is 180 degrees. Where the raster value is 0, a further analysis to define the best azimuth according to the representative day is required.

These three main results will be shown in the TOC under the same layer group.

10. Final step is to compute the results about the variation of azimuth according to the representative day and create the second layer group in the TOC. Here the function “Best_Azimuth_180_Month” takes the dictionary coming out from step 6 (each layer has cell values, for instance, in a range from 0 to 200 depending on the best azimuth values computed). Each layer in the dictionary is added by “1”. The second input of the function is the layer produced in the previous step storing the value of 180 valid for all the year. This layer is reclassified (SAGA reclassifygrsvalues) and “180” value is now 0 and all the other cells take value 1.

Each monthly layer in the dictionary (azimuth values + 1) is multiplied with the second input layer (“0-1”) and “1” will be subtracted from the final output layer. The mathematical trick is explained in the Table 4.4 with an example: every cell in [A] which overlaps a cell with 0 value in [B] means that is located in a portion of the area where 180 is the best azimuth all over the year and get “-1” as final value, all the other cells in [A] which, at the end of the mathematical process, have back the original value (overlapping with “1”) are located in those portion of area where it was

Table 4.4: [A] a layer of the 12 stored in the dictionary and [B] the best azimuth 180 layer

A (Azimuth)	C = A + 1	D = B (0-1) * C	D - 1
0	1	0	-1
178	179	1	0
180	181	0	-1
181	182	179	178
		0	-1
		181	180
		0	-1
		182	181

necessary to compute the best azimuth. In this way the model creates the 12 final monthly outputs showing portions of area where 180 is always the best azimuth and other areas where the proper azimuth value is shown.

The Figure 4.3 shows the diagram of the last steps of the script.

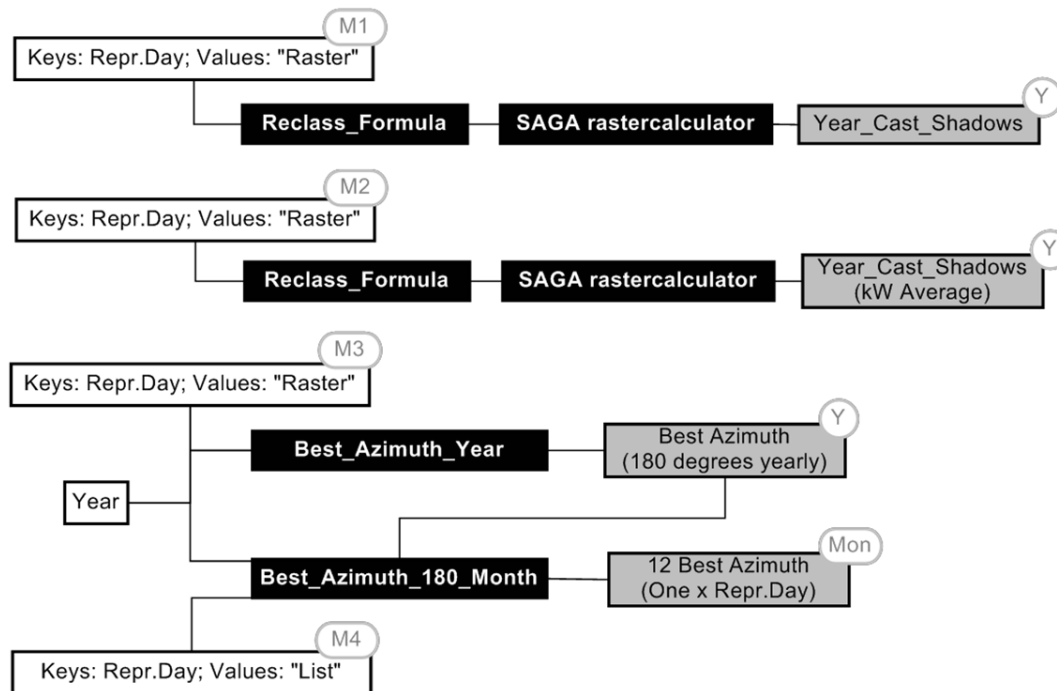


Figure 4.3: Diagram of the last steps of the main script “MAIN.py” (out of the loop). “Y” stands for “yearly result” and “Mon” for “monthly result”.

4.1.2 Function “Cast_01Rec_AzimRec”

The script of this function is a “for loop” which runs through a range starting from 1 till the floor of day-light length (called “z”) and each step within the loop is determined by a value of local time from sunrise to sunset. Each local time is defined by the formula:

$$LT = SunriseTime + z * day_step$$

Equation 4.1: Local time definition (time event)

(these input values are described in Subsection 4.1.1 point 2). For each local time, together with the representative day information, the minor function “SunPos” is called (the physical assumptions of the function are described in Section 2.2). SunPos computes for each local time the Sun azimuth and the Sun elevation and these two variables, together with the input DSM, are the main input of the SAGA tool “analyticalhillshading” (see Subsection 3.2.1). This QGIS tool, set in “Ray Tracing” mode, can produce a raster layer which shows how the shadows cast on the surface according to the sun position in the sky and tall structures on the surface of Earth. The output raster is then reclassified twice (SAGA reclassifygridvalues) to obtain the “0-1”

layer (0 = light; 1 = shadow) and the “0-Azimuth value” (0 = light; Azimuth value = shadow).

4.1.3 Function “kW_Shadow”

This function has as main input the dictionary storing “0-1” layers and local time for a given representative day originated by “Cast_01Rec_AzimRec” and the dictionary from “Month_Avg_Solar_Rad_H”. The function has a main “for loop” going through the first dictionary.

A single layer from the first dictionary is taken into consideration and, via the module GDAL (see Subsection 3.2.3), the function counts the number of cells storing “1” value and the total number of cells of the raster (the minor function “RasPixelAreaProp” provides the area occupied by each pixel in the correct units of surface) and the proportion of shaded area upon the total area is computed. Again, from the first dictionary the local time is taken and the closest time in the SMHI elaborated data is selected. Each time value in the SMHI data is coupled with a value of kWh/m², and this value will be assigned to the “1” cells of the current raster layer through a reclassification (SAGA reclassifygridvalues). Now the raster stores “0” where the surface is supposed to be shaded and the proper kWh/m² value where it is enlighten (see Section 6.1 for the discussion of this assumption). Out of the main loop, the function starts to fill in a dictionary where the key is the azimuth value and the value is the raster just reclassified.

To get the daily layer showing the total amount of kW reaching the ground, a simple raster sum is performed (SAGA rastercalculator) through all the layers stored in the main dictionary filled out of the loop.

4.1.4 Function “Best_Azimuth”

Among the major functions, “Best_Azimuth” required the most effort in programming and it is also the most time consuming part of the whole program. In Table 4.5 the definition of the input variables is presented.

Table 4.5: Input variable definition

Variable name	Description	Origin (from)
Month_Layer_Cast_Azim	Dictionary (Keys: Azimuth; Values: Raster path) Cast Shadow Δ Sun Azimuth (0: light; Azimuth value: Shadow)	Cast_01Rec_AzimRec
Day_Percentage_Shadow	Raster path: Monthly (Representative Day) Cast Shadow Percentage (0-100%)	Month_Shadow
Month_Perc	List: Monthly (Representative Day) Cast Shadow Percentage (0-100%)	Month_Shadow
%_MAX	Maximum value for the percentage range	Main input
%_MIN	Minimum value for the percentage range	Main input
Day	(representative day)	
Month	(representative day)	
Year		

The main assumption behind the function regards the so-called “percentage range”. The idea is that for areas that are shaded for more than a certain percentage value along a day are not suitable for energy production and with the same principle in areas which are shaded less than a certain value it is possible to install PV panels directly oriented towards south. In the literature there are many articles about the shadow effect affecting the energy production from PV panels (Alam et al. 2012; Guerriero et al. 2014) but exact values of percentage shading are not available so the percentage range was set arbitrarily, during the implementation phase, to 55-85%. The behaviour of the model has been tested with different minimum and maximum values of range. The procedure is presented below:

1. In a loop through the values stored in Month_Perc the function takes a percentage value and compares it to %_MAX and %_MIN making the analysis summarized in the next table (Table 4.6):

Table 4.6: Reclassification rules of the Day_Percentage_Shadow raster

If:	Day_Percentage_Shadow reclassification (SAGA reclassifygridvalues)		
	Old value	New value	Meaning
% value < %_MIN	Cell value = % value	180	Areas suitable for PV panel installation and the best azimuth is 180
	Cell value ≠ % value	0	
% value > %_MAX	Cell value = % value	0,001	Areas not suitable for energy production
	Cell value ≠ % value	0	
%_MIN < % value < %_MAX	Cell value = % value	1	<i>Additional analysis required</i>
	Cell value ≠ % value	0	

For each result (dict. value) coming from the three different “if statement” a new dictionary, with the percentage value as key is created (diagram of this step is shown in Figure 4.4).

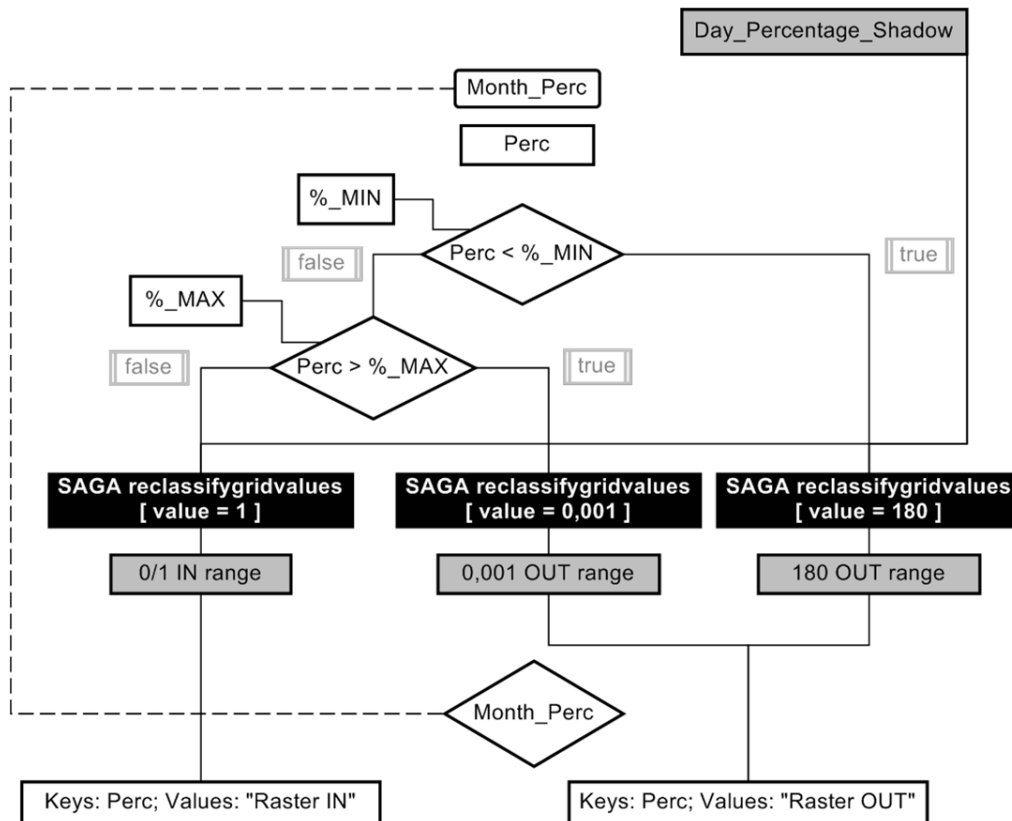


Figure 4.4: Diagram of the first steps of the script “Best_Azimuth.py” involving the “if statements”

2. The dictionary storing layers “0-1”, regarding those percentages of shadow falling into the percentage range, comes into another loop. This is a sort of “key” analysis and it is graphically explained in Figure 4.5. At each round of the loop, a layer in the dictionary is taken (e.g. Figure 4.5B). This layer is multiplied (SAGA rastercalculator) with the layers stored in the dictionary Month_Layer_Cast_Azim (e.g. Figure 4.5C) one by one. The result is that where there is “0” in the first layer, “0” is defined also in the output, where there is “1”, this number is multiplied with that value stored in the second raster (that is the Sun Azimuth value that casts the shadow at a given local time; e.g. Figure 4.5D). For every new layer coming out from this map algebra analysis the function counts the number of cells storing the current sun azimuth value and stores this number, as value, into a dictionary where the key is the azimuth angle.
3. From the previous dictionary (key: sun azimuth; value: number of cells), the function performs a weighted arithmetic mean (Equation 4.2) where the value “x” is the sun azimuth and the correspondent weight “w” is the number of cells computed in the previous step.

$$\bar{x} = \frac{\sum_{i=1}^n w_i x_i}{\sum_{i=1}^n w_i}$$

Equation 4.2: Weighted arithmetic mean formula to compute the average sun azimuth position

A new dictionary is filled with key the daily percentage of shadow and as value the result of the equation.

4. An additional loop takes the dictionary storing the layers falling into the percentage range (from step 2) and the dictionary from step 3. Here there is a mathematical assumption: if most of the shadow-covering along a day, for a given portion of area, comes when the sun has a certain average value of azimuth, then the best azimuth should be computed from the following formula:

$$180 + (180 - \text{weighted_mean_sun_azimuth})$$

Equation 4.3: Formula to compute the best azimuth orientation of a PV structure

For each layer, now with the average sun azimuth as cell value, is computed the best azimuth according to the formula in Equation 4.3 and reclassified (SAGA reclassifygridvalues) with this new value.

5. Final step is to sum (SAGA rascalculator) all the reclassified layers with the proper best azimuth value both from the percentages out and in the range. For the current representative day, for each different daily percentage of shadow the layer stores the proper best azimuth angle of orientation if a PV panel array and/or building is planned to be installed/built.

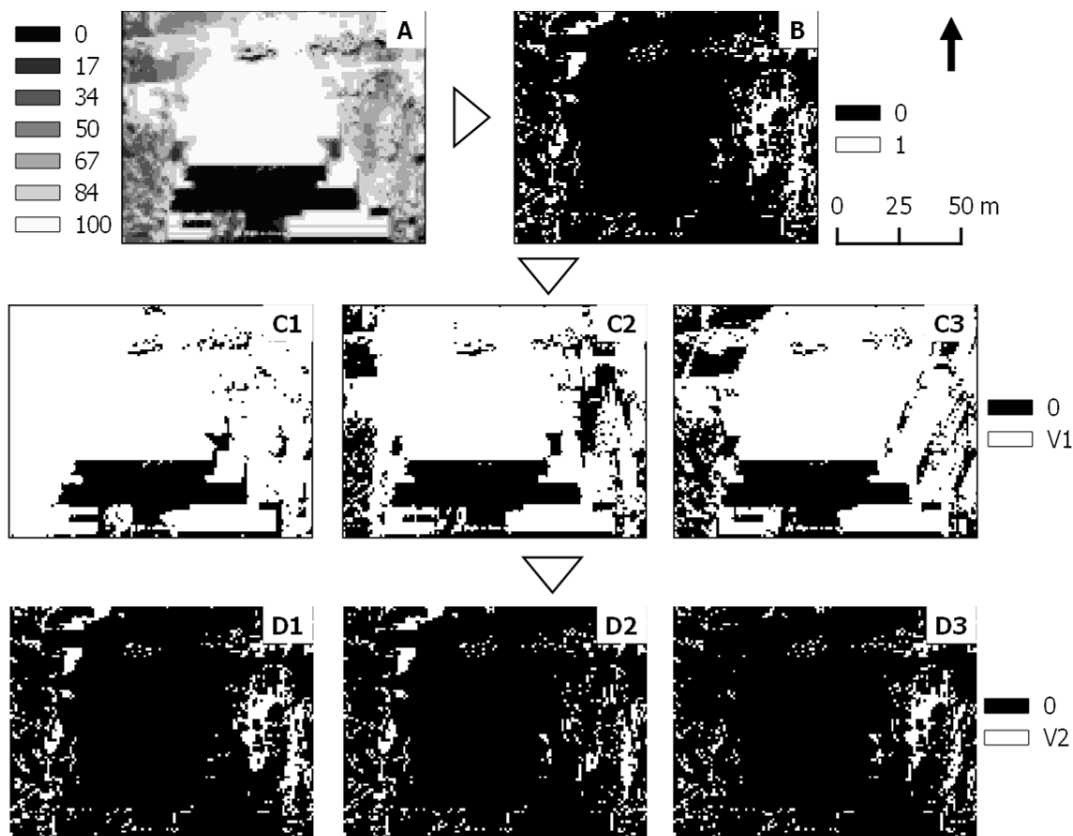


Figure 4.5: Graphical explanation of the key analysis performed by Best_Azimuth.
A: Daily shadow percentage (Legend: shadow % - 0%: full light; 100% full shadow)
B: 67% shadow (Legend: 0-light, 1-shadow)
C: shadow casting when sun azimuth (degrees) is 1: 141,52; 2: 172,13 and 3: 203,77.
(Legend: 0-light, V1-correspondent sun azimuth value)
D: results from Map Algebra. $D1=B*C1$, $D2=B*C2$ and $D3=B*C3$.
(Legend: 0-no matching, V2- correspondent sun azimuth value)

4.2 Brief description of model outputs

The model description mentions all the main output provided at the end of its execution. In a group of folders, created automatically by the program, are preserved the results shown in the main window of QGIS. All the output layers are stored by default as “.tif” file.

The colour palettes with which the various results are loaded in the TOC of QGIS are predefined within the program itself. The management of the display takes place thanks to the classes provided by the module “PyQT4”.

The program also provides text files as output. These files contain data relating to the simulation performed. The file “year_MAIN_Analysis_LOG.txt” provides general information such as the year of the analysis and the coordinates of the area. Then it lists the representative days and for each provides the date, the number of JDN, the sunrise and sunset and the respective azimuth of the Sun and the number of daylight hours. This

file is filled in directly by the main script through the values coming out from the function “RiseSetSpan” and “SunPos”. For each representative day listed are displayed the names of other three files that can be consulted: “*year.month_Sun_Angles.txt*”, “*year.month_Best_Azimuth_Info.txt*” and “*year.month_kW_Shadow_Loss_Info.txt*”.

The file “*year.month_Sun_Angles.txt*” shows the number of time-events computed per day, together with time and Sun position (elevation angle and azimuth), by the function “Cast_01Rec_AzimRec”. The file “*year.month_Best_Azimuth_Info.txt*” is filled in by the function “Best_Azimuth”. Here the user can find the list of percentage values computed within the representative day. For each single percentage value falling into the range (Subsection 4.1.4), it can be found the number of shadowed cells, created from a certain Sun azimuth value, overlapping that area percentage. Finally, the best azimuth value for each percentage is provided. The last file “*year.month_kW_Shadow_Loss_Info.txt*” provides an estimate of loss of energy due to the presence of shade. Values shown in this file come from the computation done by the function “kW_Shadow”.

5 RESULTS: A CASE STUDY

This section presents the results obtained from the model, applied to a certain area of the town of Lund, in the form of case study. As explained in Chapter 4, the model provides as output raster layers and text files containing several data about the analysis. Because of the many output layers, especially those relating to the monthly analysis, only some of them are shown as example.

The model takes into account the DSM in its total extent without distinctions of categories such as “roof“, “roads” or, in fact, “green areas”. In addition, at the time, it is not available/accessible information about, for example, a roof where it is forbidden to install PV panels or areas lacking facilities where it is planned to build. This brief consideration should be taken into account for the analysis and interpretation of the results.

The program was run on a selected study area (Section 5.1). For selected simulation year, which is the 2015, equinoxes are March 20 (spring; JDN 79) and September 23 (autumn; JDN 266) and the solstices are June 21 (summer; JDN 172) and December 22 (winter; JDN 356). Some basics information about the simulation are provided by one of the output text files, as shown in the following Table 5.1 and some technical information on Table 5.2.

**Table 5.1: Information output from the text file “2015_MAIN_Analysis_LOG.txt”.
Latitude 55,696; Longitude 13,225; year 2015; no legal hour considered**

Representative Day	JDN	Sunrise (hh:mm:ss)	Azimuth Rise (degrees)	Sunset (hh:mm:ss)	Azimuth Set (degrees)	Light Span (hh:mm:ss)
January, 17	17	08:25:19	127,47	16:11:35	232,72	07:46:16
February, 16	47	07:30:59	111,31	17:14:22	248,76	09:43:23
March, 16	75	06:21:51	93,30	18:12:49	267,71	11:50:58
April, 15	105	05:04:27	71,58	19:12:55	288,62	14:08:27
May, 15	135	03:57:51	53,76	20:11:40	306,48	16:13:49
June, 11	162	03:25:18	44,39	20:50:01	315,75	17:24:42
July, 17	198	03:47:42	48,55	20:39:38	311,42	16:51:55
August, 16	228	04:41:20	63,86	19:42:06	296,05	15:00:45
September, 15	258	05:38:55	83,89	18:26:28	276,21	12:47:33
October, 15	288	06:37:34	104,55	17:08:58	255,52	10:31:24
November, 14	318	07:39:42	122,28	16:04:08	237,32	08:24:26
December, 10	344	08:24:46	131,72	15:36:09	227,84	07:11:24

Table 5.2: Technical information about the simulation and input variables

Technical Data	Simulation Date	2015.07.01
	Called functions	All
	Number of months	12
	Execution time	32 m 8 sec
	Disk Space Amount	1,22 GB
	Reference System	SWEREF99 13 30
Input variables	Input DSM	Lund_DSM_3020_Hotel.tif
	Percentage range	55-85%
	Latitude	55.695707 N
	Longitude	13.224896 E
	Year	2015

The division of the chapter in sections follows ideally the output categories. Section 5.1 presents an overview of the study area and why it has been chosen. In Section 5.2 the layer group about yearly results is described and the same in the Section 5.3 for the monthly (representative days) outputs. An additional Section (5.4) is presented to show the test to check the behaviour of the function “BestAzimuth” at varying of the percentage range. Section 5.5 presents another additional test about the program behaviour changing the input DSM extent.

5.1 Study area

To test the model, an area within the town of Lund was chosen that had essentially two features: i) the presence of a building higher than those surrounding and ii) the presence of an area free of structures. The first condition allows appreciating the shadow effect across the time of the day. The presence of a non-built surface can be considered as an area where it is possible to build in the future.

The location of the chosen area, compared to Lund, is shown in Figure 5.1A (in the red circle). Compared to the road level (28m AMSL), the HotellScandic Star (Figure 5.1B; star-shaped building, bottom centre) fulfils the first requirement: the roofs of the building range from 15 to 25 m, the building east of the hotel which develops roughly from N to S is high about 16 m while all others do not exceed 7 m. The empty surface in the N-E corner of the study area fulfils the second assumption.

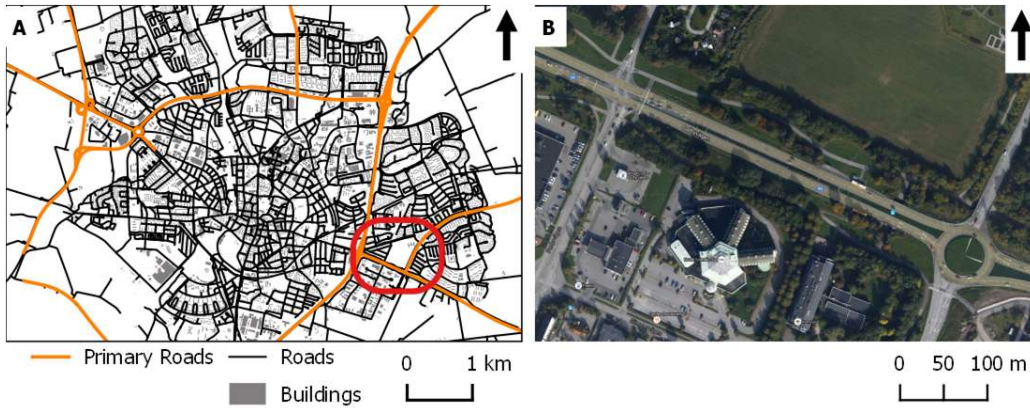


Figure 5.1: Simulation study area. A) Location within the town of Lund; B) Satellite image (Google)

The DSM of the study area (Figure 5.2; in Figure 5.3 a 3D visualization) was created from 4 LAS files, whose main characteristics are given in the following table (Table 5.3):

Table 5.3: Original LAS files used to extract the study area

LAS file SWEREF 99 13 30	Number of points	Min x(m) y(m) z(m)	Max x(m) y(m) z(m)
61745_1325.las	5 605 177	(132500.0) (6174500.0) (-51.0)	(132999.9) (6174999.9) (61.1)
61745_1330.las	4 489 982	(133000.0) (6174500.0) (-18.5)	(133499.9) (6174999.9) (72.8)
61750_1325.las	4 339 069	(132500.0) (6175000.0) (25.0)	(132999.9) (6175499.9) (151.7)
61750_1330.las	4 722 272	(133000.0) (6175000.0) (22.3)	(133499.9) (6175499.9) (156.6)

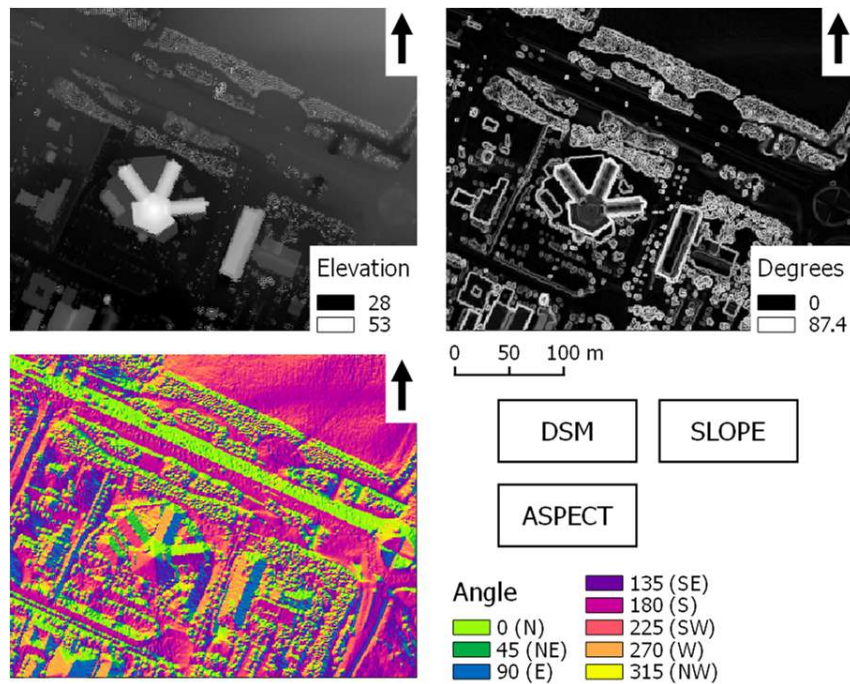


Figure 5.2: Study area DSM (elevation in meters), slope and aspect

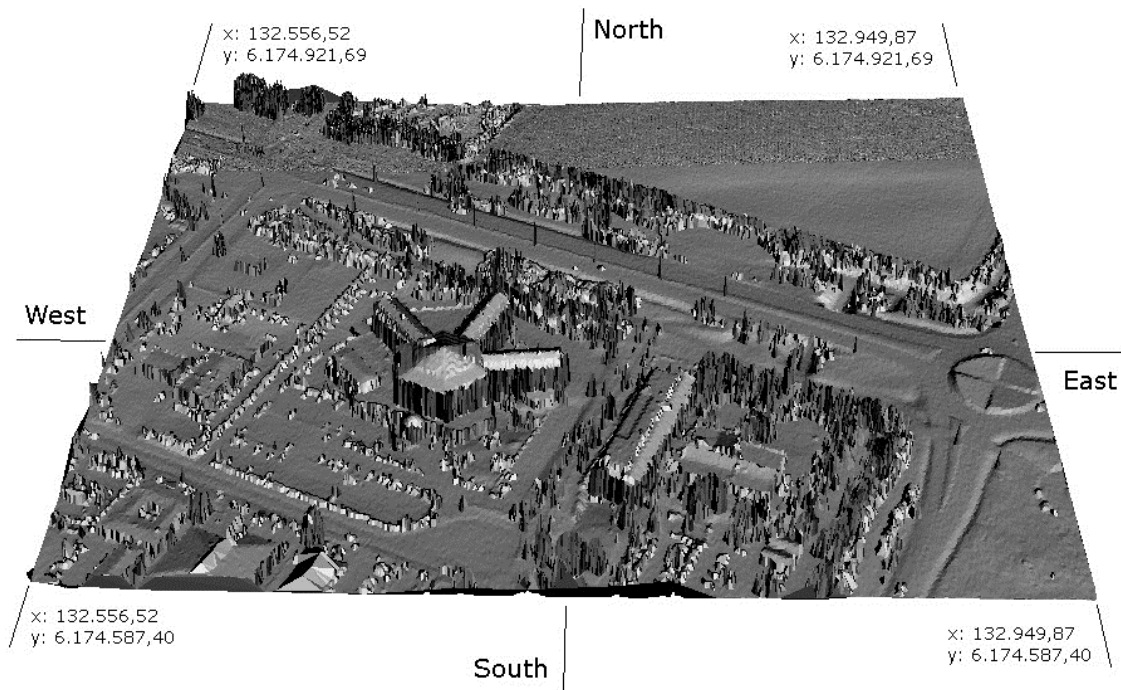


Figure 5.3: 3D visualization of the study area from the “point cloud” (created with “lasview” and modified by the author with GIMP 2.8). Reference System: SWEREF99 13 30

In the next two sections all the results provided by the model will be taken into consideration. As mentioned above, the model provides graphical results directly in the main window of QGIS and some additional text files. The layers shown are automatically grouped into two groups in the table of content (TOC): one that collects the annual output and the other gathering monthly ones.

5.2 Yearly analysis

In the first group in the TOC (named by default “Output” plus the year) the three main outputs of the study area are shown to the user.

5.2.1 Shadow casting

The first layer shown in the group presents the annual shadowing percentage (Figure 5.4) computed for the study area.

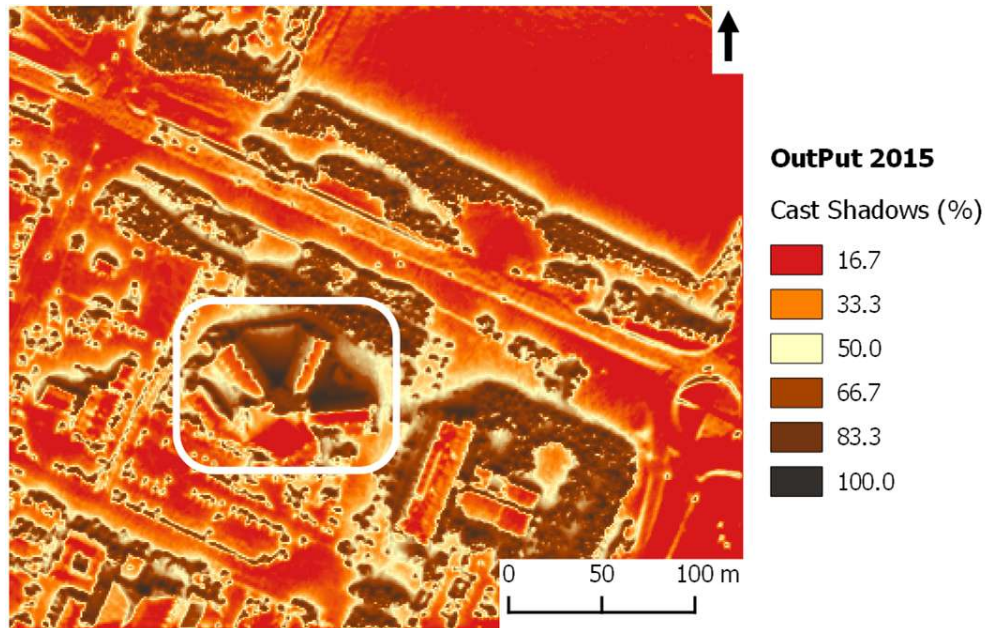


Figure 5.4: Yearly shadow casting percentage.

From the sum of the intermediate results of the 12 representative days, the final result shows the shadow distribution over a year and, as expected, the highest percentage of shadow falls behind buildings or trees (facing north direction). The highest values of shading, very closed to 100%, can be observed in the inner parts of the HotellScandic star (Figure 5.4, white frame). The same result is created with a spotted pattern in the areas covered by vegetation but that are not relevant, in order to identify areas suitable for the installation of PV panels.

As mentioned above, the area of this case study has not been chosen at random because it showed a fairly extensive portion of surface free of structures (Figure 5.4 area N-E). This area, but also others as roads, shows values of shading between 0 and 16.7%. Intermediate shade values are found in all those areas to the limit with facilities or plants, the same structures that cast shadows in different ways depending on the time of day and consequently on the angle of sun-elevation and azimuth.

5.2.2 Average kW of sun energy hitting the surface

The second yearly output shows the average amount of kWh/m² of sun energy (Figure 5.5) which hits the ground according to the data from the SMHI. As explained, values come from an additional analysis of data collected through 21 years (1980-2000) from the Swedish Meteorological Agency (SMHI).

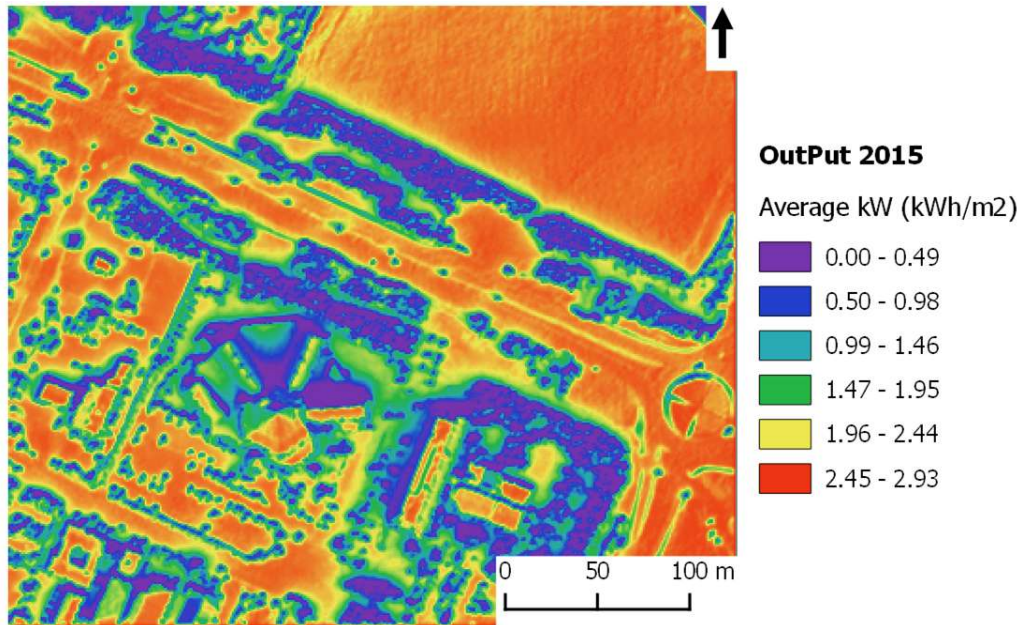


Figure 5.5: Yearly average kWh/m² of sun energy (kWh value weighted for the area represent by the pixel: 1 pixel = 1 m²)

According to the way the model was built, this result and the previous one are closely linked. In areas that are more illuminated during the year, they show greater values of solar energy. However, unlike other models for the calculation of the solar radiation (Nguyen and Pearce, 2010; Kodysh et al. 2013) here it is proposed a result as a function of historical data. Areas with a slope close to zero (Figure 5.2, up-right) and not largely involved in phenomena of annual shading or structures tilted towards south (Figure 5.2, down-left) show the highest irradiation values.

Below some layers of intermediate results (representative days) are shown (Figure 5.6). These outputs allowed the model to build up the previous end result (Figure 5.5). The winter months are characterized by a lower irradiation and, because of the lowest solar elevation during the hours of light, by shadows that stretch more. In addition, because of the azimuthal values more narrow, some areas never have the opportunity to be enlightened. This situation weighs heavily on the variation of solar energy that reaches the ground during a full calendar year.

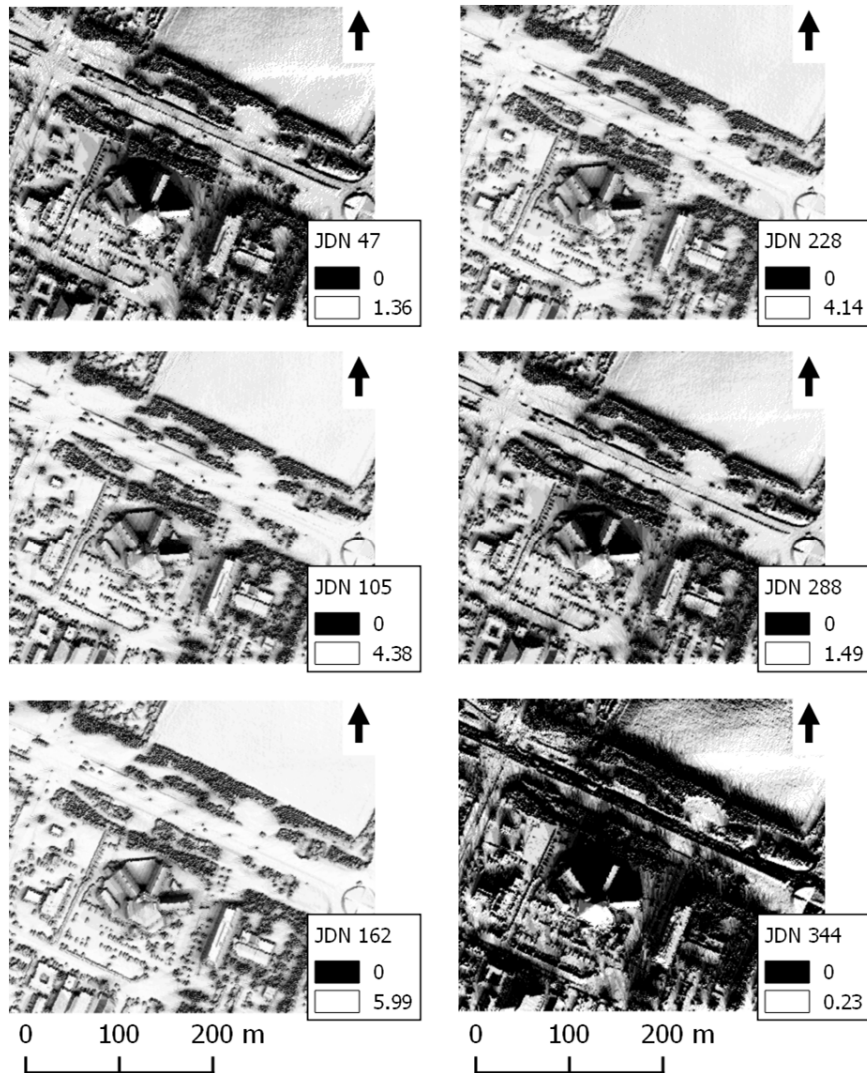


Figure 5.6: Average daily kWh/m² (representative day). JDN 47 = 16.02; JDN 105 = 15.04; JDN 162 = 11.06; JDN 228 = 15.08; JDN 288 = 16.10; JDN 344 = 10.12. Legends indicate the min and max daily average kWh/m².

5.2.3 Best yearly azimuth angle: 180 degrees

In the group of the yearly results it is presented the layers showing the areas of the DSM where, regardless of the possible month of interest, the best azimuth angle value is 180 degrees. This result means that the orientation of a new building in an empty area or the installation of an array of PV panels should occur facing directly southward. Taking into account the consideration done at the beginning of this chapter, this result (Figure 5.7) shows in green colour those areas where 180 degrees is best angle orientation from January to December.

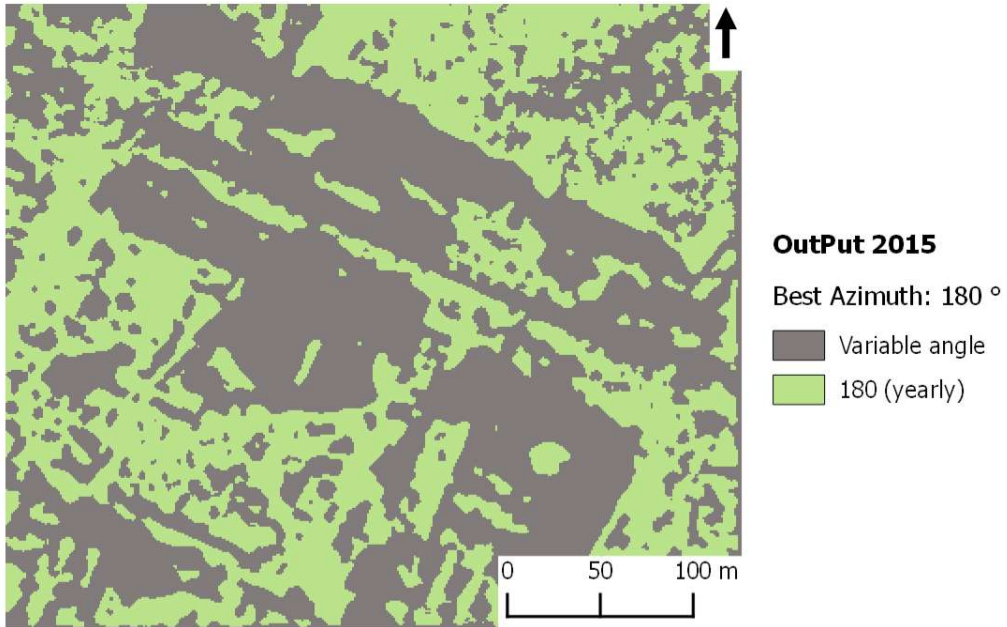


Figure 5.7: Areas where yearly best azimuth is always 180 degrees

This main output is the result of an analysis through the 12 intermediate results performed in the main “for loop” written in the main program but, as expected, this pattern is very closed to the “best azimuth” output computed for the month with the shortest light span (in this simulation the month of December, Figure 5.8)

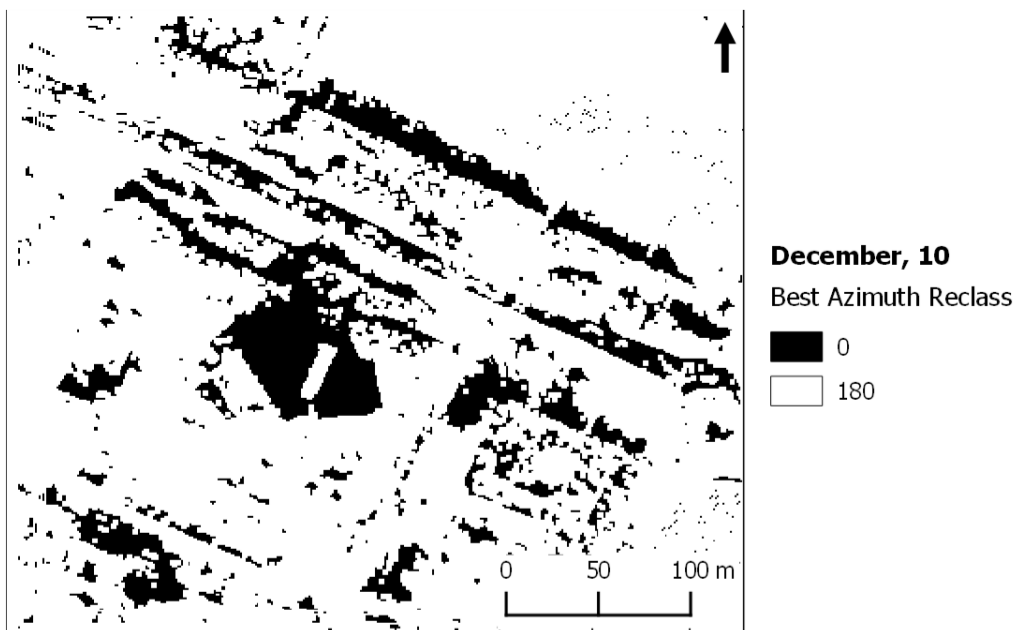


Figure 5.8: December best azimuth (JDN 344) intermediate output

The result shows a grey area (Figure 5.7) as counterpart of the green. This area is where the azimuth angle values are not always 180 degrees: values vary according to the month. This part will be presented more in detail in the following Section 5.3.

5.3 Monthly analysis

In the second group in the TOC (named by default “Output Month”) the 12 outputs, one for each representative day, about the variation of azimuth angles are shown.

Within the group there are 12 layers (Figure 5.9). Each monthly result can be considered a further elaboration of the best annual result of the azimuth angle (Figure 5.7): the area representative of the best azimuth defined in 180 degrees remains unchanged; however the area defining previously variable values (grey colour) is shown now in detail. It has been chosen, for graphical reason, to displaying the main QGIS window the azimuth values categorized in a range scale in order to show integer values to the user.

This layer group should be observed as a whole to see how the best azimuth values vary. Within the area of variability again, areas where the best value is always 180 degrees for a representative day are identified. Approaching the summer months starting from January (JDN 17), or rather toward the summer solstice (June 21, 2015; JDN 172), the value 180 degrees (“180 monthly” in the legend), or closed to it, covers a growing area, reaching a peak in the simulation, for the representative day of June (11; JDN 162) and then decreasing until JDN 344 (winter solstice for 2015: 22 December; JDN 356). The opposite behaviour can be seen if we take a look at the areas covered by 0 (we remind that 0 means that the area is not suitable for PV panels installation), approaching the summer solstice, the area decreases to increase again towards December.

The model provides results of azimuth, in the case they are not exactly facing south, which tend to get closer to 180 degrees for each representative day.

In the Figure 5.9 it is also appropriate to observe the change of the pattern of the areas. In an area where is potentially possible to install a photovoltaic system and this one is falling in a grey area of the Figure 5.7 the user can see how vary the value of best azimuth along the year. The behaviour of these areas follows, with the shade due to slightly different values of azimuth, the same behaviour previously described.

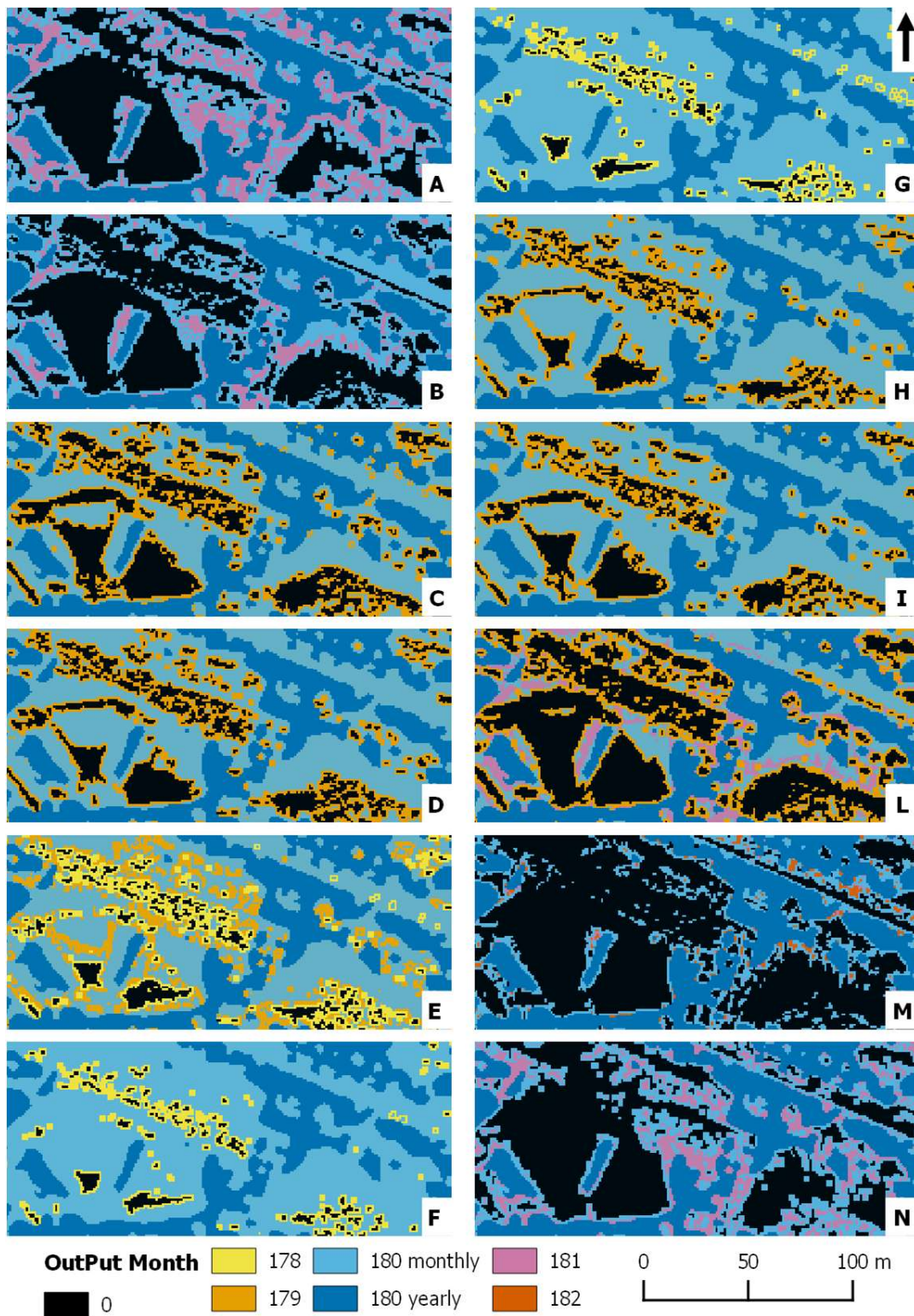


Figure 5.9: Monthly best azimuth (JDN A: 17, B: 47, C: 75, D: 105, E: 135, F: 162, G: 198, H: 228, I: 258, L: 288, M: 318, N: 344). In the legend the values of azimuth (degrees). The areas shown in the pictures are not the whole area, but an enlargement to allow a better view

5.3.1 Text outputs

In parallel with graphical results, the model creates also some text files (“txt” extension) to store additional information. Among the three text files already presented in Section 4.2, the files named “Year.Month_Best_Azimuth_Info.txt” provides more detailed information about the intermediate values of azimuth angles. In those files, gathered and summarize in the Table 5.4, there are the exact values of azimuth angle computed in the simulation for each percentage of shadow falling into the defined percentage range. The table shows an additional column reporting the number of shaded raster layers computed (“Time Events”): longer is the day light period, higher is the number of time events where the “SAGA Analytical Hillshading” module has been run. Consequently the representative days belonging to the months closer to the summer solstice will have a higher number of percentage values of “shadow casting”.

Table 5.4: Best azimuth angle values for each percentage within the percentage range (55-85%)

Representative Day	JDN	Shadow (%)	Best Azimuth (degrees)	Time events
January, 17	17	66,67	181,21	6
		83,33	180,13	
February, 16	47	62,50	181,37	8
		75,00	180,49	
March, 16	75	60,00	180,56	10
		70,00	179,62	
April, 15	105	80,00	179,48	13
		61,54	179,40	
May, 15	135	69,23	179,12	15
		76,92	179,39	
June, 11	162	60,00	179,27	16
		66,67	178,68	
July, 17	198	73,33	180,20	15
		80,00	179,82	
August, 16	228	56,25	180,48	14
		62,50	178,95	
September, 15	258	68,75	180,67	11
		75,00	180,63	
October, 15	288	81,25	180,00	9
		60,00	178,89	
November, 14	318	66,67	180,61	7
		73,33	180,38	
December, 10	344	80,00	180,28	6
		57,14	180,40	

From the previous table (Table 5.4), the suggested azimuth values coming out from the model start from a minimum value of 178,68 (JDN 135) to a maximum of 181,39 (JDN 318).

For each representative day another text file provides the information about all the percentage values computed. In the following table (Table 5.5) the content of this file is reported.

Table 5.5: Shadow percentage per representative day (text file output)

Representative Day	JDN	Percentages (%)
January, 17	17	0,00 – 16,67 – 33,33 – 50,00 – 66,67 – 83,33 – 100,00
February, 16	47	0,00 – 12,50 – 25,00 – 37,50 – 50,00 – 62,50 – 75,00 – 87,50 – 100,00
March, 16	75	0,00 – 10,00 – 20,00 – 30,00 – 40,00 – 50,00 – 60,00 – 70,00 – 80,00 – 90,00 – 100,00
April, 15	105	0,00 – 7,69 – 15,38 – 23,08 – 30,77 – 38,46 – 46,15 – 53,85 – 61,54 – 69,23 – 76,92 – 84,62 – 92,31 – 100,00
May, 15	135	0,00 – 6,67 – 13,33 – 20,00 – 26,67 – 33,33 – 40,00 – 46,67 – 53,33 – 60,00 – 66,67 – 73,33 – 80,00 – 86,67 – 93,33 – 100,00
June, 11	162	0,00 – 6,25 – 12,50 – 18,75 – 25,00 – 31,25 – 37,50 – 43,75 – 50,00 – 56,25 – 62,50 – 68,75 – 75,00 – 81,25 – 87,50 – 93,75 – 100,00
July, 17	198	0,00 – 6,67 – 13,33 – 20,00 – 26,67 – 33,33 – 40,00 – 46,67 – 53,33 – 60,00 – 66,67 – 73,33 – 80,00 – 86,67 – 93,33 – 100,00
August, 16	228	0,00 – 7,14 – 14,29 – 21,43 – 28,57 – 35,71 – 42,86 – 50,00 – 57,14 – 64,29 – 71,43 – 78,57 – 85,71 – 92,86 – 100,00
September, 15	258	0,00 – 9,09 – 18,18 – 27,27 – 36,36 – 45,45 – 54,55 – 63,64 – 72,73 – 81,82 – 90,91 – 100,00
October, 15	288	0,00 – 11,11 – 22,22 – 33,33 – 44,44 – 55,56 – 66,67 – 77,78 – 88,89 – 100,00
November, 14	318	0,00 – 14,29 – 28,57 – 42,86 – 57,14 – 71,43 – 85,71 – 100,00
December, 10	344	0,00 – 16,67 – 33,33 – 50,00 – 66,67 – 83,33 – 100,00

5.4 Changing the percentage range

The function to define the best azimuth angle requires, among other input variables, the values of maximum and minimum range within which calculate the angle according to the origin of the shadows during the course of the day. This section briefly discusses the behaviour of the model in response of this range variation.

Two simulations were performed: one with a percentage range of 45-90% and the second with extremes of 35-95%. The Table 5.6 presents the azimuth values obtained for each percentage of shadow from the two simulations together with the first (55-85%).

Table 5.6: Best azimuth values for 45-90% and 35-95% simulations across the 12 representative days. Values written in “italic” belong to all three ranges, in “normal” to 45-90 and 35-95, in “bold” only to 35-95 (data from text file output)

Representative Day (JDN)	Shadow (%)	Best Azimuth (degrees)	Representative Day	Shadow (%)	Best Azimuth (degrees)
January, 17 (17)	50,00	181,85	July, 17 (198)	40,00	180,09
	<i>66,67</i>	<i>181,21</i>		46,67	180,93
	<i>83,33</i>	<i>180,13</i>		53,33	180,81
				<i>60,00</i>	<i>178,89</i>
				<i>66,67</i>	<i>180,61</i>
				73,33	<i>180,38</i>
February, 16 (47)	37,50	180,88	August, 16 (228)	80,00	<i>180,28</i>
	<i>50,00</i>	<i>181,20</i>		86,67	179,73
	<i>62,50</i>	<i>181,37</i>		93,33	179,91
	75,00	180,49		35,71	181,35
	<i>87,50</i>	180,00		42,86	180,35
				50,00	180,11
March, 16 (75)	40,00	180,62	September, 15 (258)	<i>57,14</i>	<i>180,40</i>
	50,00	180,40		64,29	<i>179,29</i>
	<i>60,00</i>	<i>180,56</i>		71,43	<i>179,34</i>
	<i>70,00</i>	<i>179,62</i>		78,57	<i>180,09</i>
	<i>80,00</i>	<i>179,48</i>		85,71	179,86
	90,00	179,98		92,86	179,81
April, 15 (105)	38,46	179,29	October, 15 (288)	36,36	180,20
	46,15	179,43		45,45	179,87
	53,85	181,12		<i>54,55</i>	<i>180,20</i>
	<i>61,54</i>	<i>179,40</i>		63,64	<i>179,79</i>
	<i>69,23</i>	<i>179,12</i>		72,73	<i>179,45</i>
	76,92	179,39		<i>81,82</i>	<i>179,63</i>
May, 15 (135)	92,31	179,83	November, 14 (318)	90,91	179,8
	84,62	179,62		44,44	181,55
	80,00	179,82		<i>55,56</i>	<i>181,04</i>
	86,67	179,57		66,67	<i>180,97</i>
	93,33	179,65		77,78	<i>180,00</i>
				88,89	179,94
June, 11 (162)	37,50	180,41	December, 10 (344)	50,00	182,36
	43,75	180,10		<i>66,67</i>	<i>181,54</i>
	50,00	181,41		83,33	<i>180,49</i>
	<i>56,25</i>	<i>180,48</i>			
	<i>62,50</i>	<i>178,95</i>			
	68,75	180,67			

For each representative day, depending on the range defined in the simulation, to the percentages of shadow are assigned values of best azimuth that can vary. In the following figure (Figure 5.10) the comparison among the three different monthly outputs for the February 16 is shown (analogous results are obtained for other representative days). By varying the percentage range (increasing the maximum and decreasing the minimum) areas “180 yearly” and “0” contract in size and the area where it is necessary to calculate the best azimuth increases. For a better graphical comprehension, closed azimuth values are represented in the Figure 5.10 with the same colour (in detail, 180,00 and 180,49 fall in 180,0; 180,88, 181,20 and 181,37 into 181,0; raster values are correct)

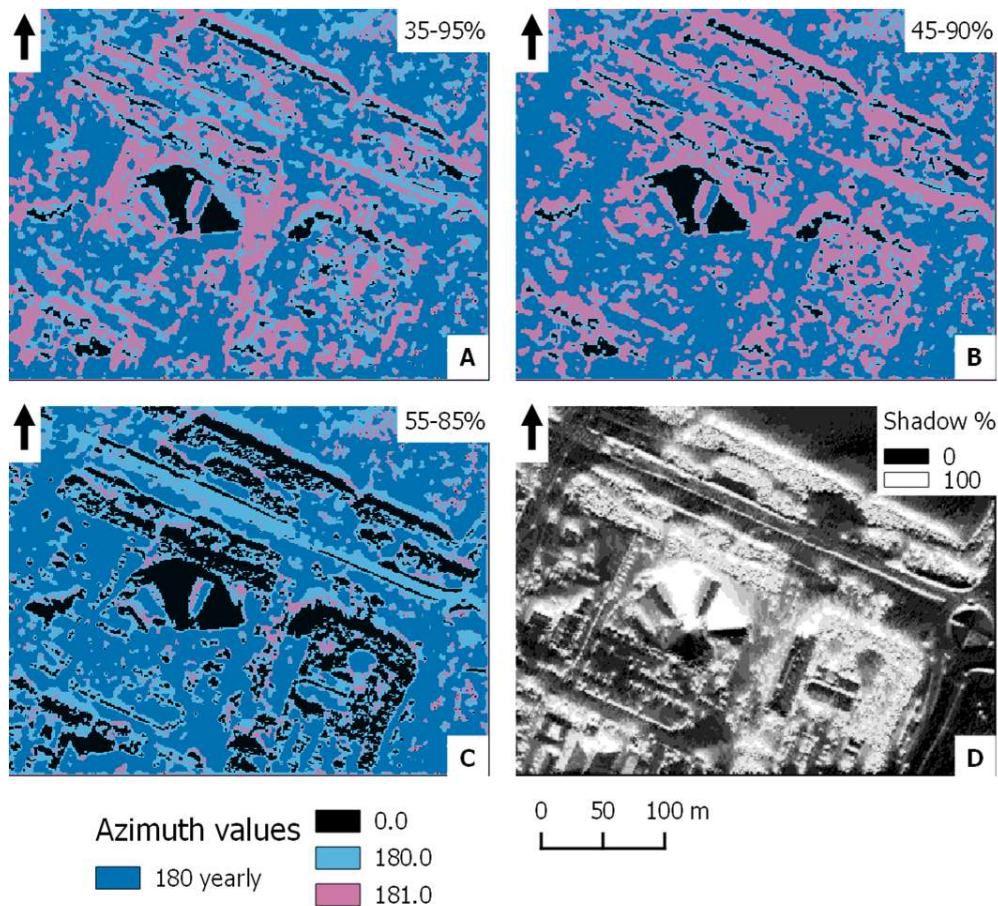


Figure 5.10:A different monthly output due to different percentage ranges (JDN 47).
A: range 35-95%; **B:** range 45-90%; **C:** range 55-85% and **D:** daily shadow casting

5.5 Changing the input DSM extension

In this last section of the chapter results from an additional test are shown. Here we tested the model to understand its behaviour in response to a change in the input DSM extent. In the next chapter we will discuss this result.

This test was designed observing the results obtained previously. The hypothesis is that different factors affect the monthly final results:

1. raster size (extension);
2. location of a structure of interest within the input raster

By the way the model was built, higher is the raster extension bigger is the influence to the best azimuth computation due to surfaces out of a possible area of interest.

On one hand it is expected to get best values of azimuth in a neighbourhood of 180 degrees, on the other hand, immediately next to tall structures are expected values of azimuth more divergent than those found in previous simulations. The assumption is that immediately near to tall structures, the radiation from the sun when it is at 180 degrees of azimuth (around noon) is shaded and then it is better to change the orientation of a PV panel array (Sun et al. 2012) to access a greater irradiation during other hours of the day. This assumption is valid for particular positions and in this test, to see how the model responded, the input DSM (Figure 5.1) was reduced in extension and the largest part of it is now occupied by the HotellScandic Star (Figure 5.11), where some peculiar areas are present (e.g.: triangle-shaped areas behind the hotel, facing north).

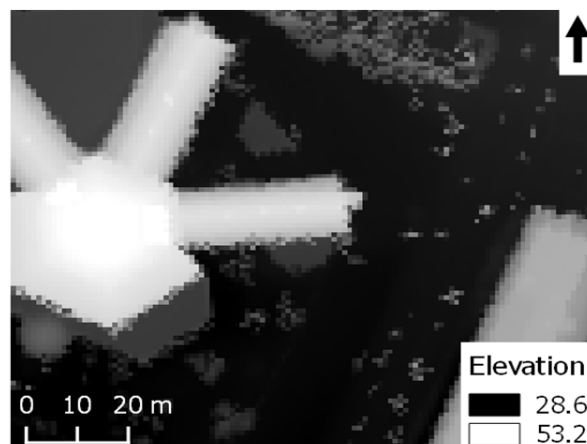


Figure 5.11: New resized input DSM

Also for this simulation text files as output were obtained, and in the following table (Table 5.7) results are reported. The suggested azimuth values coming out from the model now start from a minimum value of 176,97 (JDN 162) to a maximum of 185,22 (JDN 288).

Table 5.7: Best azimuth angle values, computed on the new input DSM, for each percentage within the percentage range (55-85%)

Representative Day	JDN	Shadow (%)	Best Azimuth (degrees)	Time Events
January, 17	17	66,67 83,33	182,71 180,51	6
February, 16	47	62,50 75,00 60,00	185,04 181,29 184,48	8
March, 16	75	70,00 80,00	179,80 179,19	10
April, 15	105	61,54 69,23 76,92 60,00	182,74 179,11 178,56 182,56	13
May, 15	135	66,67 73,33 80,00	181,28 179,32 178,49	15
June, 11	162	56,25 62,50 68,75 75,00 81,25 60,00	182,36 183,55 181,36 178,25 176,47 183,04	16
July, 17	198	66,67 73,33 80,00	182,54 178,09 177,12	15
August, 16	228	57,14 64,29 71,43 78,57	183,67 181,98 178,49 179,74	14
September, 15	258	54,55 63,64 72,73 81,82	183,99 182,24 179,16 178,77	11
October, 15	288	55,56 66,67 77,78	185,22 183,83 179,58	9
November, 14	318	57,14 71,43	184,73 183,62	7
December, 10	344	66,67 83,33	183,10 180,86	6

The 12 outputs shown in the TOC, in the monthly layer group, are shown in Figure 5.12.

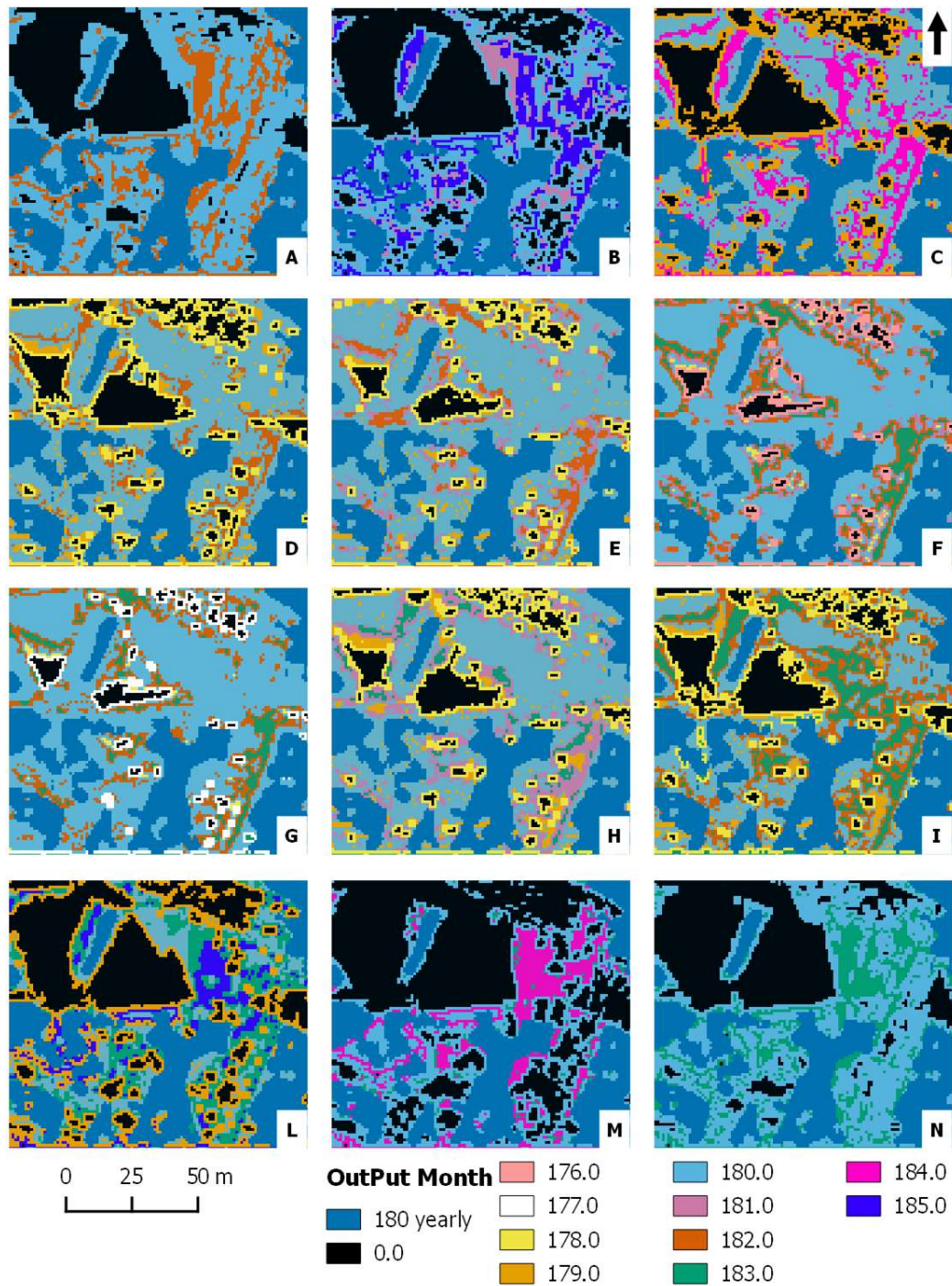


Figure 5.12: Monthly best azimuth (JDNA: 17, B: 47, C: 75, D: 105, E: 135, F: 162, G: 198, H: 228, I: 258, L: 288, M: 318, N: 344) computed on the new input DSM. In the legend the values of azimuth are expressed in degrees.

6 DISCUSSION

The practical activity carried on within the Lund Municipality for about three months has allowed creating a model to provide a solution to some of the needs of the municipality itself.

6.1 Model implementation

The main objective, the creation of a simple model through the programming language Python, has placed its bases on some physics concepts related to the apparent motion of the Sun (Chapter 2). To obtain the output results, some programming solutions and assumptions have been sought in order to take into account the geographical nature of the input data. In this subsection these solutions and assumptions will be discussed.

The main program (Subsection 4.1.1point 9), after having performed the analysis through the 12 representative days, defines the area where the best azimuth is always 180 degrees. Here a filter is used to eliminate pixels with isolated values with respect to those around. Here the assumption is that if a pixel represents an area of 1 m² or less and that cell has for instance a value of 0 among cells showing values of 180, it may be more appropriated to consider it as a part of the main 180 area and make that area more homogeneous. This assumption has also a more practical justification: a PV panel structure often requires a minimum area in order to amortise, in a defined time, the total costs with the production of electricity. Obviously there are many variables to consider about the characteristics of the PV panels, latitude and/or energy costs and it is not the aim of this thesis, but with little information it is possible to get an order of magnitude to estimate a minimum area. A PV system with a nominal power ≤ 10 kW is sufficient for residential or small business uses (Feldman et al. 2014). The electricity production per square meter varies, among other things, also as a function of the materials (Jardine and Lane 2003), however a general rule of thumb is 1 kW = approximately 8 m² of PV panel area. Taken into account these considerations, it is reasonable to filter the layer in order to eliminate individual pixels, if not even to groups of 4 or 8, according to the area represented by the pixel itself.

In the Subsection 4.1.2 is described the function “Cast_01Rec_AzimRec” which shows, for every given time along the day, how the shadows cast on the surface. The function operates with a time step variable of about one hour going from a minimum of 6 time events up to 16 (Table 5.4). This variable has been defined in this way to suit the needs of time for the computation: each time event corresponds to the creation of a different raster. It is possible to increase or decrease the number of computations by the modification of the parameters “z” and “day_step” in Equation 4.1. Increase the computational phase of this function; however, it would have an impact on the timing on

all other functions that use the outputs of “Cast_01Rec_AzimRec” as input parameter. In addition to this consideration about computational time demand, it is useful to remember that the data used on the global radiation supplied by the SMHI have hourly intervals and for this reason it seemed more correct to perform the elaboration on a time interval of about one hour.

The function “kW_Shadow” described in Subsection 4.1.3 is based on the assumption that when the light, coming from the sun, hits the ground then the value of potentially usable kW is assigned according to the historical data or, more in general, to a sun radiation model output (Suri and Hofierka 2004). In the shaded areas instead it is assumed that the value of potentially usable kW collapses to zero; clearly it is a simplification but shadows and environmental temperature are among the variables that most influence the efficiency of a PV panel (Verso et al. 2015). In the model, the shadow is considered as a factor strongly limiting and the temperature is not taken into account. The shadow, however, has to do with the efficiency of the photovoltaic panels in a particular way due to how the panels themselves are designed. That the casting of a shadow on one or more PV panels can be a problem is quite intuitive. The PV panels convert sunlight into electricity but when a panel, or part of it, is not illuminated, it produces little energy or does not produce it at all. Actually the matter is worse, because in almost all cases, the single panel is part of a parallel connected string, called “block” (Pveducation.org 2015d), that reflects the overall loss in production of the shaded panel even if only a portion of the block is shaded (Section 2.4; Díaz-Dorado et al. 2010). Ultimately it makes sense to simplify and considered “0” the energy production of a shaded panel rather than defining a formula which estimates the loss of production as a function of the current degree of shading.

The implementation of the model, as seen, has several assumptions that take into account both physical laws and computational limits. These assumptions had allowed writing the program in order to get a result in a reasonable time and to be based on a simple but essentially correct physical model. Now we will discuss the most important assumption: how to define the value of best azimuth within the defined percentage range.

As described above (Subsection 4.1.4) for each percentage of shadow, within a single representative day, an azimuth value is provided. The method developed to determine this value sees the calculation of a weighted average (Equation 4.2) among all values of solar azimuth along the day: in practice it defines which is the influence of the shadow due to each individual position of the sun (varying the time events) on the calculation of the total daily percentage (Figure 4.5). With this assumption it is possible to initially obtain the single value, so it is necessary to calculate an average, of the azimuth angle of the sun from where it is mainly projected the shadow and later with the simple Equation 4.3 to define the angle of orientation that can “escape”, turning in the opposite direction compared to the value of 180 degrees, from the position more subject to shading. The behavior of the model, in the light of this assumption, it was also tested with varying the percentage range and extent of the DSM (Sections 5.4 and 5.5).

The model was tested for three different percentages range to evaluate its behaviour (35-95%, 45-90% and 55-85%). From the model it was expected that, to vary the size of

the range, the output values of best azimuth were always in a neighbourhood of 180 degrees even for the new percentage now included into the new, larger range. Comparing the values in the Table 5.4 and Table 5.6 the prediction has been fulfilled. The single values of azimuth refer to a precise percentage within the representative day, and enlarging the percentage range, increase the number of percentages that require the intervention of the function “Best Azimuth” to assess the best angle of orientation. The values of percentage daily, falling always in all three ranges, will always show the same value of azimuth. A final consideration: greater percentage values of shadow (85, 90 and 95) also have their azimuth values which tend to 180 degrees, however it should be considered that greater percentage values should be excluded because too exposed in the shade (hence the definition of the percentage range with a maximum) and then they would be areas where a PV panel could not operate with good efficiency.

Finally, the model was tested on an input DSM with a lower extension if compared with the original and where the tallest structure was highly decentralized. As mentioned in the results (Section 5.4), decreasing the extent of the study area, the calculated range of azimuth values increases from a range between 178,68 and 181,39 for the DSM in Figure 5.2 to a range between 176,47 and 185,22 for the DSM in Figure 5.11. This is due to a sort of flattening of the values closer to 180, increasing the extension of the input DSM. In general it seems to make more sense to limit the analysis in the proximity of the area of interest, in this case the model returns values that interpret better the phenomenon of shading due to the structures that affect almost exclusively the area taken into consideration by providing angular values more extremes regardless facilities further away than have no effect. This measure was also used by Kodysh and colleagues (Kodysh et al. 2013) that in their work have used a buffer of 25m around roofs to consider only those structures that shade the roof taken into consideration.

The summer months (JDN: 135, 162 and 198) deserve a final consideration. In Figure 5.12, for these months, the best azimuth value 180 is close to the structure of the hotel but there is to consider that at noon of the summer months the sun elevation is higher and thus can make the azimuth to tend towards that value.

6.2 Model output results

6.2.1 Yearly results

The first annual result provided by the model is the layer of the “shadow casting”. The analysis provides an overall picture of dark areas that are most represented in the portions of the surface behind higher structures. This analysis requires an additional consideration closely related to the origin of the input data: the DSM created from files originated with LiDAR technology. The presence of plants on the surface is an aspect that needs to be taken into account carefully. As mentioned in Subsection 3.1.1, the DSM of the town of Lund comes from a point cloud created in two flight-sessions between mid-January and mid-February of 2015. In this period, at the latitude of Lund, the deciduous plants have no leaves yet, but the trunks and branches are not transparent to the LiDAR technology (Lu et al. 2014). Same consideration is even truer for evergreens plants or fully-closed canopies. The DSM, created from data collected in the winter period, was then subject to

an annual round analysis, so even in months where the state of development of the plants was no longer representative of the real situation. In the detail of the case study area, where the plants are deciduous, this means that there may be an underestimation of the shadow generated in the summer months because of the plants with full leaf coverage and hence highest and/or more dense. In each case it should be taken into consideration the chosen resolution of the raster (1m) and the interpolation automatically done by LAStool (Subsection 3.2.3) which, again, can modify a little the DSM respect to reality.

The situation of Lund and in general in places at high latitudes is peculiar because, in the days between the two equinoxes (March 20 and September 23 for the year 2015), the sun rises and sets with azimuth angles which are smaller day by day (considering the north azimuth as 0 degrees). This situation allows some areas, which seem to be apparently unreachable by the sunlight, to become illuminated and therefore the presence of shadow at percentages close to 100% during the whole year is real only in special situations such as that shown for the building in Figure 5.4.

The second layer belonging to the annual results shows a daily average of kWh/m² (Figure 5.5) calculated on the year of the analysis. The input data about the kW of energy coming from the Sun does not come from a physical model but from real data collected by the SMHI. Also this result is closely related to the previous one about shadows percentage. It has been decided to consider this result as part of the analysis of the year (2015), however, it has to be considered that SMHI data are available for two decades from 1980 to 2000. This choice is dictated by the fact that the analysis of the shadows instead is also a function of the chosen year.

Using historical data rather than rely on a model is essentially justified by two reasons: i) this type of historical data is nowadays more and more available and ii) a physical model to calculate these values, only for a single day, often takes some time to perform the analysis. Available historical data often covers an extended time series and in this way also the variation of weather conditions that affect kW actually reaching the surface is indirectly incorporated. On the other hand however, the use of a physical model requires the knowledge of parameters that are not equally easy to retrieve for the area of interest. Also different models can require different parameters and can give slightly different results. This specific part of the model (Subsection 5.2.2) allows the inclusion of upgrades in the data regarding kW: here were available those from 1980 to 2000 but data collected in other years can be used.

In the following subsection the third annual result will be discussed together with the monthly results.

6.2.2 Best azimuth and monthly results

The last annual result draws the portion of the area of interest where 180 degrees is the best azimuth value across all the year. As highlighted in the previous chapter, this result (Figure 5.7) is visually similar to that of the shorter representative day in the computation of hours of light (Figure 5.8). This similarity was expected. The area of best azimuth at 180 degrees in the shortest day among the 12 considered, will be shared to all the other

11 while, among these last, the portions at 180 degrees outside the area defined in green colour in Figure 5.7 will be part of the variable area (Figure 5.9; it is necessary to stress once again that the values shown visually in the legend are rounded to the integer values of best azimuth to improve reading).

Coming back on how the model was built, the script within this phase of the process performs a final step where a filter is passed through the layer to return a more homogeneous result as already expressed in the previous section. This step was necessary for a possible further development of the model: to consider a minimum area where is suitable to install a PV array and/or roof footprint (Section 2.4). In that case, a solitary pixel (in this case representing a square meter) could not fit a minimum area requirement.

Ultimately according to the model there is, as expected, a change in the azimuth values across different JDN, but these changes are not very pronounced, are in the order of ± 2 degrees compared to 180 (Figure 5.9). However the most informative perspective, even for practical purposes, it is to see how areas vary on equal azimuth value. An installed PV panel can move along the azimuth plane within a limited angle range but may be sufficient, it is more important to know if this energy structure is installed in an area where it is necessary to adjust this angle during the year to make the most of solar radiation.

6.3 Further insights on the theoretical background of the model

The developed model presented in this report has as key analysis that one presented in Subsection 4.1.2 (Function “Cast_01Rec_AzimRec”) to obtain the pattern of the shadows for each representative day. As can be seen from the description of the analysis, and from Figures 4.5, this process is based solely on the trigonometric relationship that is created between the rays emitted from a source of light with a given position (defined by the values α and φ , respectively elevation and azimuth angles) and structures that rise from the surface of the area under study (DSM). The QGIS tool “SAGA Analytical Hillshading”, run in “Ray tracing” mode, processes geometrically shadows without taking into account the possibility that between the source of light and the objects that rise from the surface there may be something that prevents the light to outline clearly the shadows on the ground. Staying on the geometric basis of the model, whenever “SAGA Analytical Hillshading” is used, this produces a result as if the component of solar radiation, present at that given time-event, was direct, that is, with a sky completely clear of clouds and therefore without the diffuse component of the solar radiation. However this consideration is important in the model presented here when we want to move from a purely geometrical basis of the relationship between the source of light and objects on the ground to the physical and meteorological basis. In the northern hemisphere of the Earth, the diffuse solar radiation is greater at high latitudes than at lower latitudes and, typically, places located at the most high latitudes are also the most affected by cloud cover. In addition, the percentage of solar radiation that is diffused tends to be greater in winter than in summer. In this way, the ratio of direct and diffuse solar radiation varies greatly between winter and summer, especially at high latitudes (Starr and Palz 1983; Parding et al. 2014). Therefore the analysis of the shadows should take account of this situation. In this sense it would be appropriate to deepen the knowledge about the weather of the area

of interest and, in parallel, creating an *ad hoc* function that can handle at least the cloud cover in order to better redefine those time-events in which it is likely to consider the solar radiation only in its direct component. This possible refinement of the model would have repercussions on the other important application analysis: the process of defining the value of best angle orientation. In the presence of diffuse radiation, the orientation of the PV panel is of marginal importance for the production of electric energy because the definition of the best position for a PV panel has meaning only in relation to direct light rays (more intense) and not for those refracted in different directions. With the diffuse radiation, the light rays come from different directions and also carry less energy compared to a bundle of direct light rays hitting a PV panel and in this sense also the production of electricity would be significantly affected almost to make the panel inefficient.

The impact that can have, in the various analyses, the presence of direct or diffuse radiation also affects the average annual solar radiation hitting the area of interest. The SMHI provides hourly values of global radiation and in this way would be more informative to have an input dataset where are presented data collected separately for direct and diffuse radiation. This would allow to be able to calculate the fraction of energy hitting the ground, arising for instance only by the diffuse radiation.

7 CONCLUSIONS AND FURTHER DEVELOPMENTS

The production of electricity from renewable and non-polluting sources is an area that sees more and more investment and is of interest not only for individuals, but also for the governments and agencies. Energy from the sun is one of these sources and to use it efficiently it is compulsory to consider several variables both physical and technological. In this short experience we wanted to create a model that, taking into account a small set of these variables, could provide some results preparatory for a possible use of solar energy.

The model developed here is based on input data of increasingly easy availability: the data on solar radiation are often made available by the national energy agencies or by meteorological centers and the digital terrain models (or data allowing their creation) are becoming more commonly used and freely available. The model has also been created entirely using FOSS software and packages available online at no additional charge. This approach is justified by the need, for many administrations, to reduce costs and at the same time to respond effectively to requests that these recent years posed, especially on delicate issues such as environmental.

The model, by definition, is a simplification of the reality that, availing of a limited number of variables, tries to provide a correct and usable result for some purposes. In our case the model provides essentially three kinds of graphics results and some text files with data. The first two results are annual and, in the area of interest, show the percentage of shadow casting and an estimation of the sun energy hitting the ground according to some data provided by the SMHI. The third result, which is the most important, is about the best orientation of an energy structure such as a PV panel: the model present a pictorial result showing the portion of area where this value is always 180 degrees and a series of twelve pictorial outputs, one for each representative day, where the user can see the areas where this angular value requires an adjustment.

This model is always questionable and improvable, both in its basic assumptions and in the programming and already during its implementation have emerged interesting insights. Thanks to these insights, the behavior of the model has been tested with varying of percentage range and extent of the input DSM. The percentage range allows the user to define *a priori* which is the minimum percentage of shading beyond which the best azimuth value is always 180 degrees and maximum beyond which it would make no sense to install a PV panel. It has also been changed the input DSM extent input to understand how the model answered always about the best values of azimuth: the higher the extent of the DSM, decreases the range of the best azimuth. This behavior has allowed understanding that it is more appropriate to carry out this analysis on a DSM extent which is only slightly larger than the area of interest.

Insights raised during the implementation have highlighted other aspects that can improve the model in future. Always reconnecting to the extent of the input DSM, it would seem that the general orientation of the buildings or structures within the area of interest may affect the values of best azimuth. This debate is based on a purely visual analysis: buildings oriented more towards NE-SW lead to values of best azimuth on average less than 180degrees; if the orientation is in the opposite direction (NW-SE) values would be greater than 180. This consideration needs to be investigated. In any case, to choose the correct extent of the study area could obviate this effect.

As has often been said, the variables that can be considered are many and it is necessary to make choices, but some may be internalized in the model for the analysis improvement without having to intervene excessively on the work already done. A first value that can be inserted in the model is the minimum area of a PV panel: in this way it would be possible to identify those portions of the area which are not sufficiently large to accommodate an energy structure. This possibility is closely related to the matter on the elimination, through the filtering, of those pixels storing values different from surroundings cells. This model carries out the analysis, in a general sense, both for the installation of PV panels to be positioned at ground level and on roofs of future buildings: in the second case it would be useful to allow the user to enter the building height in design. This option would require a pre-processing of the DSM so as to provide the necessary information on the elevation of a final area not yet built. Finally it would be useful to define not only the best azimuth but also the best value of tilt angle of the PV panels: this aspect is in fact the most analysed in the literature.

The application could be improved maintaining the primary analyses unchanged, however these may be also modified taking into account the different nature of solar radiation. The analysis of the pattern of the shadows should be improved taking into account the fact that at high latitudes such as the city of Lund, the cloud cover, especially in the wintertime, has a strong impact on the amount of direct solar radiation. These changes, which go directly to the core of the application, could provide even more probable results both on the actual amount of solar radiation on the ground and on the values of best orientation of a PV panel.

Here is a final consideration of practical nature. At the moment the model lies in a set of Python files that can be called very quickly through the Python console provided by QGIS. QGIS however, allows creating a Graphical User Interface (GUI) for its GeoAlgorithms, also called “plug-in”. Translating this model into a plug-in, as well as providing a graphical interface, it would be possible to make it available to all users of the network, storing it in a separate repository of QGIS, specially created by the community with the purpose to share these tools.

REFERENCES

- Alam, N., V. Coors, S. Zlatanova, and P. Oosterom. 2012. Shadow effect on photovoltaic potentiality analysis using 3D city model. In *International Archives of the Photogrammetry, Remote Sensing and Spatial Information Sciences*, 209-214. XXII ISPRS Congress
- AL-Naimi, R., M. AL-Salihi and D. Bakr. 2014. Neural network based global solar radiation estimation using limited meteorological data for Baghdad, Iraq. *International Journal of Energy and Environment* 5: 79-84.
- American Society of Photogrammetry and Remote Sensing,. 2013. *LAS Specification Version 1.4 R13*. Bethesda, Maryland.
- Araya-Muñoz, D., D. Carvajal, A. Sáez-Carreño, S. Bensaid, and E. Soto-Márquez. 2014. Assessing the solar potential of roofs in Valparaíso (Chile). *Energy and Buildings* 69: 62-73. Elsevier BV. doi:10.1016/j.enbuild.2013.10.014.
- Asprs.org,. 2015. LASer (LAS) File Format Exchange Activities. Retrieved June 29, 2015, from <http://www.asprs.org/Committee-General/LASer-LAS-File-Format-Exchange-Activities.html>
- Astro.cornell.edu,. 2015. Altitude and Azimuth. Retrieved July 07, 2015, from http://www.astro.cornell.edu/academics/courses/astro201/alt_az.htm
- Bakirci, K. 2012. General models for optimum tilt angles of solar panels: Turkey case study. *Renewable and Sustainable Energy Reviews* 16: 6149-6159. Elsevier BV. doi:10.1016/j.rser.2012.07.009.
- Blom Sweden AB,. 2015. *Laserskanning Lund Redogörelse*. Sollentuna.
- Cassell, M. 2009. When local governments choose open source over proprietary software: a study of four European cities. In *Annual Meeting of the Western Political Science Association*.
- Catita, C., P. Redweik, J. Pereira, and M. Brito. 2014. Extending solar potential analysis in buildings to vertical facades. *Computers & Geosciences* 66: 1-12. Elsevier BV. doi:10.1016/j.cageo.2014.01.002.
- Chen, J., A. Hill, and L. Urbano. 2009. A GIS-based model for urban flood inundation. *Journal of Hydrology* 373: 184-192. Elsevier BV. doi:10.1016/j.jhydrol.2009.04.021.
- Chong, K., C. Wong, F. Siaw, T. Yew, S. Ng, M. Liang, Y. Lim, and S. Lau. 2009. Integration of an On-Axis General Sun-Tracking Formula in the Algorithm of an Open-Loop Sun-Tracking System. *Sensors* 9: 7849-7865. MDPI AG. doi:10.3390/s91007849.
- Díaz-Dorado, E., A. Suárez-García, C. Carrillo, and J. Cidrás. 2010. Influence of the shadows in photovoltaic systems with different configurations of bypass diodes. In *SPEEDAM 2010*, 134-139.
- Docs.qgis.org,. 2015. Print Composer. Retrieved July 10, 2015, from http://docs.qgis.org/2.0/en/docs/user_manual/print_composer/print_composer.html
- Doggett, L., W. Tangren, and S. Panossian. 1990. *Almanac for Computers*. Washington, DC: Nautical Almanac Office - United States Naval Observatory.

- Duffie, J., and W. Beckman. 2006. *Solar engineering of thermal processes*. Hoboken, N.J.: Wiley.
- El Saeid Mustafa, A. 2012. Development of a Photo Voltaic Building Rooftop Integration Analysis Tool for GIS for Dokki District, Cairo, Egypt. Master Thesis, Lund University.
- Feldman, D., G. Barbose, R. Margolis, T. James, S. Weaver, N. Darghouth, R. Fu, and C. Davidson et al. 2014. Photovoltaic System Pricing Trends: Historical, Recent, and Near-Term Projections - 2014 Edition. Presentation.
- Freitas, S., C. Catita, P. Redweik, and M. Brito. 2015. Modelling solar potential in the urban environment: State-of-the-art review. *Renewable and Sustainable Energy Reviews* 41: 915-931. Elsevier BV. doi:10.1016/j.rser.2014.08.060.
- Fu, P., and P. Rich. 1999. Design and implementation of the Solar Analyst: an ArcView extension for modeling solar radiation at landscape scales. In *Proceedings of the 19th annual ESRI user conference*.
- Gdal.org. 2015. GDAL: GDAL - Geospatial Data Abstraction Library. Retrieved July 09, 2015, from <http://www.gdal.org/>
- Gnu.org. 2015. What is free software?- GNU Project - Free Software Foundation. Retrieved July 10, 2015, from <https://www.gnu.org/philosophy/free-sw.html>
- Gopinathan, K., N. Maliehe, and M. Mpholo. 2007. A study on the intercepted insolation as a function of slope and azimuth of the surface. *Energy* 32: 213-220. Elsevier BV. doi:10.1016/j.energy.2006.04.009.
- Grass.osgeo.org. 2015. GRASS GIS manual: r.sun. Retrieved August 17, 2015, from <https://grass.osgeo.org/grass64/manuals/r.sun.html>
- Grena, R. 2012. Five new algorithms for the computation of sun position from 2010 to 2110. *Solar Energy* 86: 1323-1337. Elsevier BV. doi:10.1016/j.solener.2012.01.024.
- Guerriero, P., F. Di Napoli, F. Cominale, V. d'Alessandro, and S. Daliento. 2014. Accurate analysis of small shadows effects on photovoltaic systems yield. *2014 International Symposium on Power Electronics, Electrical Drives, Automation and Motion*. Institute of Electrical & Electronics Engineers (IEEE). doi:10.1109/speedam.2014.6872081.
- Gulin, M., M. Vašak, and N. Perić. 2013. Dynamical optimal positioning of a photovoltaic panel in all weather conditions. *Applied Energy* 108: 429-438. Elsevier BV. doi:10.1016/j.apenergy.2013.03.006.
- Hedén, P. 2013. Solelpotentialbedömning - framställning av solelpotentialkarta för Lund och utvärdering av laserdata. Master Thesis, Lunds Tekniska Högskola.
- Hetrick, W., P. Rich, and S. Weiss. 1993. Modeling insolation on complex surfaces. In *Proceedings of the thirteenth annual ESRI user conference* 2: 447-458.
- Hofierka, J., and M. Suri. 2002. The solar radiation model for Open source GIS: implementation and applications. In *GRASS users conference 2002*, 1-19. Open source GIS.
- Hofierka, J., and M. Zlocha. 2012. A New 3-D Solar Radiation Model for 3-D City Models. *Transactions in GIS* 16: 681-690. Wiley-Blackwell. doi:10.1111/j.1467-9671.2012.01337.x.
- Jafarkazemi, F., and S. Saadabadi. 2013. Optimum tilt angle and orientation of solar surfaces in Abu Dhabi, UAE. *Renewable Energy* 56: 44-49. Elsevier BV. doi:10.1016/j.renene.2012.10.036.

- Jardine, C., and K. Lane. 2003. Photovoltaics in the UK: An introductory guide for new consumers. Presentation Oxford.
- Kodysh, J., O. Omitaomu, B. Bhaduri, and B. Neish. 2013. Methodology for estimating solar potential on multiple building rooftops for photovoltaic systems. *Sustainable Cities and Society* 8: 31-41. Elsevier BV. doi:10.1016/j.scs.2013.01.002.
- Krafringen.se,.2015a. Solkartan - se hur mycket solinstrålning ditt tak har - Krafringen. Retrieved June 24, 2015, from <http://www.krafringen.se/Privat/Solceller/Solkartan/>
- Krafringen.se,. 2015b. Solkartan - om projektet - Krafringen. Retrieved June 25, 2015, from <http://www.krafringen.se/Privat/Solceller/Solkartan/Projektet-bakom-Solkartan/>
- Kumar, L., A.K. Skidmore, and E. Knowles. 1997. Modelling topographic variation in solar radiation in a GIS environment. *International Journal Of Geographical Information Science* 11:475-97
- Lamie, R., W. Campbell, and W. Molnar. 2012. The fiscal-geographic nexus: An overview of fiscal impact assessment in local policy development. *Applied Geography* 32: 54-60. Elsevier BV. doi:10.1016/j.apgeog.2010.07.007.
- Li, R., Z. Tang, X. Li, and J. Winter. 2013. Drainage Structure Datasets and Effects on LiDAR-Derived Surface Flow Modeling. *ISPRS International Journal of Geo-Information* 2: 1136-1152. MDPI AG. doi:10.3390/ijgi2041136.
- Lta.cr.usgs.gov,. 2015. Light Detection and Ranging (LIDAR). Retrieved June 25, 2015, from <https://lta.cr.usgs.gov/LIDAR>
- Lu, X., Q. Guo, W. Li, and J. Flanagan. 2014. A bottom-up approach to segment individual deciduous trees using leaf-off lidar point cloud data. *ISPRS Journal of Photogrammetry and Remote Sensing* 94: 1-12. Elsevier BV. doi:10.1016/j.isprsjprs.2014.03.014.
- Lukač, N., and B. Žalik. 2013. GPU-based roofs' solar potential estimation using LiDAR data. *Computers & Geosciences* 52: 34-41. Elsevier BV. doi:10.1016/j.cageo.2012.10.010.
- Maksimovic, Č. 2009.Overland flow and pathway analysis for modelling of urban pluvial flooding.*JHR* 47: 000. Informa UK Limited. doi:10.3826/jhr.2009.3361.
- Martinez-Rubio, A., F. Sanz-Adan, and J. Santamaria. 2015. Optimal design of photovoltaic energy collectors with mutual shading for pre-existing building roofs. *Renewable Energy* 78: 666-678. Elsevier BV. doi:10.1016/j.renene.2015.01.043.
- Melo, E., M. Almeida, R. Zilles, and J. Grimoni. 2013. Using a shading matrix to estimate the shading factor and the irradiation in a three-dimensional model of a receiving surface in an urban environment. *Solar Energy* 92: 15-25. Elsevier BV. doi:10.1016/j.solener.2013.02.015.
- Morse, P., and H. Feshbach. 1999. *Methods of theoretical physics*. Boston: McGraw Hill.
- Nguyen, H., and J. Pearce. 2010. Estimating potential photovoltaic yield with r.sun and the open source Geographical Resources Analysis Support System. *Solar Energy* 84: 831-843. Elsevier BV. doi:10.1016/j.solener.2010.02.009.
- National Oceanic and Atmospheric Administration (NOAA),. 2012. *Lidar 101: An Introduction to Lidar Technology, Data, and Applications*. Charleston, SC: NOAA Coastal Services Center.
- Oceanservice.noaa.gov,. 2015. What is LIDAR?. Retrieved June 27, 2015, from <http://oceanservice.noaa.gov/facts/lidar.html>

- Parding, K., J. Olseth, K. Dagestad, and B. Liepert. 2014. Decadal variability of clouds, solar radiation and temperature at a high-latitude coastal site in Norway. *Tellus B* 66. doi:10.3402/tellusb.v66.25897.
- Pveducation.org, 2015a. PVEducation. Retrieved Aprile 29, 2015, from <http://www.pveducation.org/>
- Pveducation.org, 2015b. Calculation of Solar Insolation | PVEducation. Retrieved July 13 2015, from <http://pveducation.org/pvcdrom/properties-of-sunlight/calculation-of-solar-insolation>
- Pveducation.org, 2015c. Introduction | PVEducation. Retrieved August 18 2015, from <http://www.pveducation.org/pvcdrom/modules/introduction>
- Pveducation.org, 2015d. Mismatch Effects in Arrays | PVEducation. Retrieved August 13 2015, from <http://www.pveducation.org/pvcdrom/modules/mismatch-effects-in-arrays>
- Python.org, 2015a. Welcome to Python.org. Retrieved April 16, 2015, from <https://www.python.org/download/releases/2.7/>
- Python.org, 2015b. Welcome to Python.org. Retrieved April 16, 2015, from <https://www.python.org/>
- Qgis.org, 2015a. Welcome to the QGIS project!. Retrieved April 16, 2015, from <https://www.qgis.org/en/site/index.html>
- Qgis.org, 2015b. Discover QGIS. Retrieved July 10, 2015, from <http://www.qgis.org/en/site/about/index.html>
- rapidlasso GmbH, 2012. LAStools. Retrieved July 09, 2015, from <http://rapidlasso.com/lastools/>
- Re.jrc.ec.europa.eu, 2015. PV potential estimation utility. Retrieved July 13, 2015, from <http://re.jrc.ec.europa.eu/pvgis/apps4/pvest.php?lang=en&map=europe>
- Renno, C., and F. Petito. 2013. Design and modeling of a concentrating photovoltaic thermal (CPV/T) system for a domestic application. *Energy and Buildings* 62: 392-402. Elsevier BV. doi:10.1016/j.enbuild.2013.02.040.
- Rigollier, C., O. Bauer, and L. Wald. 2000. On the clear sky model of the ESRA — European Solar Radiation Atlas — with respect to the heliosat method. *Solar Energy* 68: 33-48. Elsevier BV. doi:10.1016/s0038-092x(99)00055-9.
- Santos, T., N. Gomes, S. Freire, M. Brito, L. Santos, and J. Tenedório. 2014. Applications of solar mapping in the urban environment. *Applied Geography* 51: 48-57. Elsevier BV. doi:10.1016/j.apgeog.2014.03.008.
- Shamim, M., R. Remesan, M. Bray, and D. Han. 2015. An improved technique for global solar radiation estimation using numerical weather prediction. *Journal of Atmospheric and Solar-Terrestrial Physics* 129: 13-22. Elsevier BV. doi:10.1016/j.jastp.2015.03.011.
- Solangi, K., M. Islam, R. Saidur, N. Rahim, and H. Fayaz. 2011. A review on global solar energy policy. *Renewable and Sustainable Energy Reviews* 15: 2149-2163. Elsevier BV. doi:10.1016/j.rser.2011.01.007.
- Skelion. 2013. Skelion 5.1.5 user's guide
- Sketchup.com, 2015. SketchUp for Architecture | SketchUp. Retrieved August 16, 2015, from <http://www.sketchup.com/3Dfor/architecture>
- Solar Electricity Handbook, 2015. Solar Irradiance Calculator. Retrieved July 13, 2015, from <http://solarelectricityhandbook.com/solar-irradiance.html>

- Smhi.se,. 2015. Strålning | SMHI. Retrieved July 09, 2015, from Retrieved June 03, 2015, from <http://www.smhi.se/klimatdata/meteorologi/stralning>
- Starr, M., and W. Palz. 1983. *Photovoltaic power for Europe: an assessment study*. Dordrecht, Holland: D. Reidel Publishing Company.
- Strang.smhi.se,. 2015. data extraction. Retrieved June 03, 2015, from <http://strang.smhi.se/omna/>
- Sun, L., L. Lu, and H. Yang. 2012. Optimum design of shading-type building-integrated photovoltaic claddings with different surface azimuth angles. *Applied Energy* 90: 233-240. Elsevier BV. doi:10.1016/j.apenergy.2011.01.062.
- Suri, M., and J. Hofierka. 2004. A New GIS-based Solar Radiation Model and Its Application to Photovoltaic Assessments. *Transactions in GIS* 8: 175-190. Wiley-Blackwell. doi:10.1111/j.1467-9671.2004.00174.x.
- Tait, P. 2014. A critical decade for public health: responsibility for energy transitions. *Australian and New Zealand Journal of Public Health* 38: 4-6. Wiley-Blackwell. doi:10.1111/1753-6405.12187.
- Technical standard UNI 8477-1, 1983.
- Tutorialspoint.com,. 2015. Python Dictionary. Retrieved July 10, 2015, from http://www.tutorialspoint.com/python/python_dictionary.htm
- Urry, J. 2014. The Problem of Energy. *Theory, Culture & Society* 31: 3-20. SAGE Publications. doi:10.1177/0263276414536747.
- Usa.autodesk.com,. 2015. Ecotect Analysis - Sustainable Building Design Software - Autodesk. Retrieved August 16, 2015, from <http://usa.autodesk.com/ecotect-analysis/>
- Verso, A., A. Martin, J. Amador, and J. Dominguez. 2015. GIS-based method to evaluate the photovoltaic potential in the urban environments: The particular case of Miraflores de la Sierra. *Solar Energy* 117: 236-245. Elsevier BV. doi:10.1016/j.solener.2015.04.018.
- Williams.best.vwh.net,. 2015. Sunrise/Sunset Algorithm. Retrieved April 27, 2015, from http://williams.best.vwh.net/sunrise_sunset_algorithm.htm
- Yadav, A., and S. Chandel. 2013. Tilt angle optimization to maximize incident solar radiation: A review. *Renewable and Sustainable Energy Reviews* 23: 503-513. Elsevier BV. doi:10.1016/j.rser.2013.02.027.
- Ying, S., L. Li, and R. Guo. 2011. Building 3D cadastral system based on 2D survey plans with SketchUp. *Geo-spatial Information Science* 14: 129-136. Informa UK Limited. doi:10.1007/s11806-011-0483-2.
- Zijffers, J., M. Janssen, J. Tramper, and R. Wijffels. 2008. Design Process of an Area-Efficient Photobioreactor. *Mar Biotechnol* 10: 404-415. Springer Science + Business Media. doi:10.1007/s10126-007-9077-2.

APPENDICES

Appendix 1: LAS file with some information from Header Block and VLR (point data not shown)

```
lasinfo for C:/Users/049034/MODEL/fusa.laz
reporting all LAS header entries:
file signature:      'LASF'
file source ID:     0
global_encoding:    0
project ID GUID data 1-4: 00000000-0000-0000-0000-000000000000
versionmajor.minor: 1.1
system identifier:   'LAStools (c) by Martin Isenburg'
generating software: 'lasclassify (1 10920) unlicensed'
file creation day/year: 40/2010
header size:        227
offset to point data: 321
number var. length records: 1
point data format:  1
point data record length: 28
number of point records: 277573
number of points by return: 263413 13879 281 0 0
scale factor x y z:  0.01 0.01 0.01
offset x y z:        0 0 0
min x y z:           277750.00 6122250.00 42.21
max x y z:           277999.99 6122499.99 64.35
variable length header record 1 of 1:
reserved            43707
user ID             'LASF_Projection'
record ID           34735
length after header 40
description         'by LAStools of Martin Isenburg'
GeoKeyDirectoryTag version 1.1.0 number of keys 4
key 1024 tiff_tag_location 0 count 1 value_offset 1 - GTModelTypeGeoKey: ModelTypeProjected
key 3072 tiff_tag_location 0 count 1 value_offset 32754 - ProjectedCSTypeGeoKey: UTM 54 southern hemisphere
key 3076 tiff_tag_location 0 count 1 value_offset 9001 - ProjLinearUnitsGeoKey: Linear_Meter
key 4099 tiff_tag_location 0 count 1 value_offset 9001 - VerticalUnitsGeoKey: Linear_Meter
LASzip compression (version 2.0r1 c2 50000): POINT10 2 GPSTIME11 2
reporting minimum and maximum for all LAS point record entries ...
X      27775000 27799999
Y      612225000 612249999
Z      4221 6435
intensity 10 62293
return_number 1 3
number_of_returns 1 3
edge_of_flight_line 0 0
scan_direction_flag 0 0
classification 1 6
scan_angle_rank 79 103
user_data 0 197
point_source_ID 1 1
gps_time 5880.963028 5886.739738
overview over number of returns of given pulse: 249493 27232 848 0 0 0 0
histogram of classification of points:
17553 unclassified (1)
180868 ground (2)
37030 high vegetation (5)
42122 building (6)
```

LIST OF PUBLICATIONS

Institutionen för naturgeografi och ekosystemvetenskap, Lunds Universitet.

Student examensarbete (Seminarieuppsatser). Uppsatserna finns tillgängliga på institutionens geobibliotek, Sölvegatan 12, 223 62 LUND. Serien startade 1985. Hela listan och själva uppsatserna är även tillgängliga på LUP student papers (<https://lup.lub.lu.se/student-papers/search/>) och via Geobiblioteket (www.geobib.lu.se)

The student thesis reports are available at the Geo-Library, Department of Physical Geography and Ecosystem Science, University of Lund, Sölvegatan 12, S-223 62 Lund, Sweden. Report series started 1985. The complete list and electronic versions are also electronic available at the LUP student papers (<https://lup.lub.lu.se/student-papers/search/>) and through the Geo-library (www.geobib.lu.se)

- 335 Fei Lu (2015) Compute a Crowdedness Index on Historical GIS Data- A Case Study of Hög Parish, Sweden, 1812-1920
- 336 Lina Alleesson (2015) Impact of photo-chemical processing of dissolved organic carbon on the bacterial respiratory quotient in aquatic ecosystems
- 337 Andreas Kiik (2015) Cartographic design of thematic polygons: a comparison using eye-movement metrics analysis
- 338 Iain Lednor (2015) Testing the robustness of the Plant Phenology Index to changes in temperature
- 339 Louise Bradshaw (2015) Submerged Landscapes - Locating Mesolithic settlements in Blekinge, Sweden
- 340 Elisabeth Maria Farrington (2015) The water crisis in Gaborone: Investigating the underlying factors resulting in the 'failure' of the Gaborone Dam, Botswana
- 341 Annie Forssblad (2015) Utvärdering av miljöersättning för odlingslandskapets värdefulla träd
- 342 Iris Behrens, Linn Gardell (2015) Water quality in Apac-, Mbale- & Lira district, Uganda - A field study evaluating problems and suitable solutions
- 343 Linnéa Larsson (2015) Analys av framtida översvämningrisker i Malmö - En fallstudie av Castellums fastigheter
- 344 Ida Pettersson (2015) Comparing *Ips typographus* and *Dendroctonus ponderosae* response to climate change with the use of phenology models
- 345 Frida Ulfves (2015) Classifying and Localizing Areas of Forest at Risk of Storm Damage in Kronoberg County
- 346 Alexander Nordström (2015) Förslag på dammar och skyddsområde med hjälp av GIS: En studie om löv- och klockgroda i Ystad kommun, Skåne

- 347 Samanah Seyedi-Shandiz (2015) Automatic Creation of Schematic Maps - A
Case Study of the Railway Network at the Swedish Transport Administration
- 348 Johanna Andersson (2015) Heat Waves and their Impacts on Outdoor Workers
– A Case Study in Northern and Eastern Uganda
- 349 Jimmie Carpman (2015) Spatially varying parameters in observed new particle
formation events
- 350 Mihaela – Mariana Tudoran (2015) Occurrences of insect outbreaks in Sweden
in relation to climatic parameters since 1850
- 351 Maria Gatzouras (2015) Assessment of trampling impact in Icelandic natural
areas in experimental plots with focus on image analysis of digital photographs
- 352 Gustav Wallner (2015) Estimating and evaluating GPP in the Sahel using
MSG/SEVIRI and MODIS satellite data
- 353 Luisa Teixeira (2015) Exploring the relationships between biodiversity and
benthic habitat in the Primeiras and Segundas Protected Area, Mozambique
- 354 Iris Behrens & Linn Gardell (2015) Water quality in Apac-, Mbale- & Lira
district, Uganda - A field study evaluating problems and suitable solutions
- 355 Viktoria Björklund (2015) Water quality in rivers affected by urbanization: A
Case Study in Minas Gerais, Brazil
- 356 Tara Mellquist (2015) Hållbar dagvattenhantering i Stockholms stad - En
riskhanteringsanalys med avseende på långsiktig hållbarhet av Stockholms
stads dagvattenhantering i urban miljö
- 357 Jenny Hansson (2015) Trafikrelaterade luftföroreningar vid förskolor – En
studie om kvävedioxidhalter vid förskolor i Malmö
- 358 Laura Reinelt (2015) Modelling vegetation dynamics and carbon fluxes in a
high Arctic mire
- 359 Emelie Linnéa Graham (2015) Atmospheric reactivity of cyclic ethers of
relevance to biofuel combustion
- 360 Filippo Gualla (2015) Sun position and PV panels: a model to determine the
best orientation